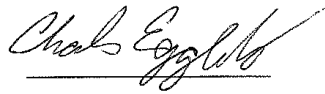APPROVAL SHEET

Title of Thesis: Simulating the effects of changes in P-selectin density on the

PMN rolling mechanics.

Name of Candidate: Grishma S. Prabhukhot

Master of Science, 2018
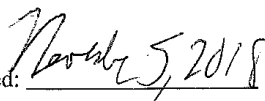
Thesis and Abstract Approved:

Dr. Charles D. Eggleton

Professor

Mechanical Engineering

Date Approved:

ABSTRACT

Title of Document: SIMULATING THE EFFECTS OF

CHANGES IN P-SELECTIN DENSITY ON

THE PMN ROLLING MECHANICS

Grishma S. Prabhukhot, Master of Science,

2018

Directed By: Professor Dr. Charles D. Eggleton

Department of Mechanical Engineering

Polymorphonuclear (PMN) leukocytes, when rolling on endothelium, undergoes deformation, the PSGL-1 molecules form bonds with the P-selectin molecules on the surface of the endothelium in a linear shear field. We have studied the effects of P-selectin density on bond formation and cell rolling mechanics using computational simulation and mathematical modelling. The PMN leukocyte is modeled as a 3-D deformable spherical capsule, in a newtonian fluid, the receptor mediated rolling of this capsule is simulated on a P-selectin coated surface. The results indicate the number of receptor-ligand bonds formed increases with an increase in the P-selectin, the rolling velocity decreases with an increase in the P-selectin density, a higher bond force is experienced by the capsule rolling on a surface with higher P-selectin density.

SIMULATING THE EFFECTS OF CHANGES IN P-SELECTIN DENSITY ON

THE PMN ROLLING MECHANICS

By

Grishma S. Prabhukhot.

Thesis submitted to the Faculty of the Graduate School of the

University of Maryland, Baltimore County, in partial fulfillment

of the requirements for the degree of

Master of Science

2018

Advisory Committee:

Professor Dr. Charles D. Eggleton(Advisor)

Dr. Rohan J. Banton (Co-advisor)

Dr. Meilin Yu

Dr. Erin Lavik

Dr. Gregory Szeto

To everyone who guided and supported

me throughout my journey.

Acknowledgements

Table of Contents

List of Tables

List of Figures

Chapter 1: Introduction

1.1 Immune system and response

ROLLING
PSGL-1 MOLECULES
LEUKOCYTE

ADHESION
MICROVILLI

FIRM ADHESION

TRANSMIGRATION

P-SELECTIN MOLECULE   ICAM MOLECULE   ENDOTHELIAL CELL

Figure 1: The Leukocyte Adhesion Cascade

The immune system responds to an alien attack of infectious bacteria by recruiting white blood cells or leukocytes out of the circulatory system and towards the site of infection. The response of the immune system follows a sequence of events irrespective of the type of leukocyte and the path of leukocytes towards the target. This sequence is often known as Leukocyte extravasation , the leukocyte adhesion cascade or alternatively also called Leukocyte diapedesis. The leukocyte adhesion cascade involves several stages; the recruitment of polymorphonuclear leukocytes (PMNs) to the site of trauma is initiated with the chemoattraction of PMN to the endothelial cell

1

surface, the chemoattraction process is then followed by rolling-adhesion, tight adhesion and endothelial transmigration. Upon detecting the infectious site, the macrophages release cytokines. Cytokines signal the endothelial cells to express selectins on their surface. Out of the various selectins, various studies suggest that the binding of P-selectin to the P-selectin glycoprotein ligand-1 (PSGL-1) mediates the very earliest leukocyte rolling during an inflammatory response (Dore et al.,1993; Mayadas et al., 1993). Upon activation, the integrins also known as the ligands bind to the receptors also known as the selectins. These bonds decreases the rolling velocity of the cell. The initial almost spherical shape of leukocyte transforms to a flat oblate spheroidal shape. The restructuring of an endothelial cell takes place allowing the transmigration of leukocyte to the site of infection or trauma.

Scientists have studied the role of P-selectin in the progression of systemic lupus-like diseases in P-selectin deficient mice; the result of which was a significant early mortality (Xiaodong He et al. 2018). Thus, deficiency of P-selectin results in failure to respond to an inflammation. This can result in leukocyte adhesion deficiency (LAD).

Normal human blood contains 4000-10,000 leukocytes/µl. They have a cytoplasmic fluid enclosed within the cell membrane along with other organelles and are covered with protrusions called microvilli. On the tips of the microvilli are the ligands such as P-selectin glycoprotein ligand-1 (PSGL-1) and L-selectin.

1.2 Literature review

Mathematically developed dynamic model by Hammer et al. 1987 is considered to be a pioneering work focusing on the behavior of cell rolling-adhesion on a surface. Using the phase plane method, they developed a biological model of cell rolling-adhesion dynamics. This 2-Dimensional model was recognized as a "point attachment model". However, this model did not elucidate the mechanics of shape change due to deformation and adhesion of entire cell under shear flow. Besides this, they had also made an assumption that the contact area is a uniform disk which was later proven to be not true. A further development was also required to model the influence of hydrodynamic forces on the cell and its transmission from the cell deformation to the forces that disrupt the receptor-ligand bonds. Later on, Hammer and Apte, 1992, developed an Adhesion Dynamics algorithm (AD) to study the behavior of leukocyte binding kinetics and rolling on a hard surface. The leukocyte was modeled as a hard sphere with rigid microvilli. The Adhesion Dynamic model was able to recreate the transient "stop and go" motion of the leukocyte and calculate the translational velocity. The kinetic rates for receptor-ligand bonds were based on the expressions calculated by Dembo et al,1994. This model simulated the effect of the number of ligands on the microvilli tips, the rate of reaction for receptor-ligand bond formation, stiffness of receptor-ligand bonds referred to as 'springs' in their paper, and the effect of hydrodynamic stresses on the cell adhesion. Following this study, Tözeren and Ley (1992) presented a biophysical model of a leukocyte as a rigid sphere rolling on a surface. The cell membrane folds and microvillus were represented with surface projections. A local stiffness parameter was introduced to mimic the phenomenon of extension of the bond length when the force on the bond is increased. They found that the bond length influenced the leukocyte rolling. In addition they also hypothesized that at a higher shear rate, the rate of bond formation is not a critical parameter that influences the cell rolling. The major drawback of this paper was that they did not account for the tension in the cell membrane when subjected to a shear flow which was important to be accounted for. Since the leukocytes are elastic in nature of rather than rigid, they undergo deformation which results in the tension in membrane.

The research evolved in a way that the domain based models were developed which included the volume of fluid and the immersed boundary method. Khismatullin and Truskey (2004) developed a 3-D viscoelastic drop model. Simulations were performed to study the deformation of a cell

bound to a substrate in a channel. Some of the drawbacks of this study were that it was conducted for a relatively small time duration of 4 ms which did not provide enough time for the cell to reach a steady state deformation. Thus, there was a need to further study the response of microvillus deformation and the cell deformation to the shear forces and the firm adhesion of the rolling leukocyte.

A 2D computational model based on including different scales pertaining to cell deformation (µm), bond length (nm) and receptor-ligand binding (nm), was constructed by (N'Dri et al., 2003). This multiscale model was designed primarily to study the cell deformability coupled with cell rolling in shear flow. The bond formation and breakage were based on the binding kinetics proposed by Dembo et al 1994. However, the major drawback of this model was that the surface roughness or surface projections of the leukocyte caused due to the presence of the microvilli were neglected. Also, the molecular bonds were assumed to be fixed on the membrane surface which is not observed in vivo. The molecular bonds are not rigid bodies, but rather deform when subjected to shear force (Bell et al, 1978). They had also assumed that the forces experienced by the cell were only transmitted by the bonds while neglecting the restoring forces. The receptor-ligand bond formation was defined by a deterministic relationship and so the jerky motion of a cell rolling on a substrate was not captured. The cell shape predicted by the compound liquid drop model of N'Dri et al. ,2003 deviated from the experimental observations. Thus, there was a need to redefine the compound liquid drop model with a 3D model which incorporated the salient features of a leukocyte. An elastic ring model by Dong et al., 1999; Dong and Lei, 2000 was developed to understand the leukocyte deformation and adhesion behavior in shear flow. This 2D model consisted of an elastic ring adhered to a substrate under fluid stresses. One of the major drawbacks of this study was the assumption of nonphysical constraints imposed on peeling length limits and on the initial cell shape. This cell shape on deformation deviates from the experimental observations.

To overcome the shortcomings of the previously described models, a more realistic model in 3D was developed (Jadhav et al. 2005; Pawar et al.2008; Pappu et al 2008; Gupta et al. 2010). The leukocyte was represented having an unstressed spherical shape initially, enclosing a Newtonian fluid in a thin hyperelastic membrane. The cell could deform in 3D when subjected to adhesion and/or hydrodynamic forces present when rolling in a linear shear field (Jadhav et al. 2005). This

is a domain-based immersed boundary method (IBM) (Peskin and McQueen, 1989). The model parameters were chosen to represent PSGL-1 mediated PMN rolling on a P-selectin coated substrate. The binding kinetics of receptor-ligand interactions (Dembo, 1994) were simulated by using the Hookean spring model. This model predicted the bond formation and rupture on a stochastic approach rather than a deterministic simulation. This stochastic approach was simulated by using the Monte Carlo method (Hammer and Apte,1992; King and Hammer, 2001). This model was further extended by Pawar et al. 2008 by incorporating microvillus deformability. The cell rolling characteristics were studied with respect to the cell deformation, microvillus deformation, and receptor-ligand binding kinetics.Balsara et al. 2015 used the Immersed boundary method with the Finite element method and the Mooney Rivlin constitutive relationship to investigate the influence of strain hardening of the cell membrane on cell deformation, rolling and binding kinetics. The effect of unstressed reverse rate was observed on the receptor-ligand binding kinetics. A dimple was observed to form at the cell-substrate contact surface as opposed to a contact area that is a uniform disk (Hammer et al. 1987).

However, the role of leukocyte rolling on a substrate coated with controlled density of P-selectin is yet to be explored thoroughly. Chia Hua-Lee et al.,2010 conducted an experiment of patterning the P-selectin on substrates to study the motion of HL60 cells. HL60 cell line is a diseased cell line commonly found in patients with acute promyelocytic leukemia, these cells possess the PSGL-1 ligand on the tips of microvilli. Through this experiment, they showed that it was possible to control the ability of HL60 to roll and that the patterning affects the rolling velocity. This study was extended further by Bose et al. 2013 wherein they demonstrated flow fractionation of leukocytes interaction with P-selectin patterned on a surface in an asymmetric fashion. This study was done to analyze the cell separation process and in an interest to use the cell separation for developing point-of-care tests. Primarily the research described earlier studied the rolling behavior of leukocytes with a view to achieving cell separation effectively. However, in order to understand the rolling behavior, we must take into account the previously described computational models. These computationally developed models have explained the influence of deformation and binding kinetics on the cell along with the rolling of the cell.

Thus, besides these in vitro experimental studies, in Pappu et al., 2008, modeled the leukocytes as a hyperelastic microcapsule filled with Newtonian fluid computationally. Their hyperelastic

membrane was modeled based on the Neo-Hookean constitutive relations and its binding kinetics were explained using the Hookean spring approach. These microcapsules were made to interact with a selectin coated hard surface. In 2006 Rachik et al. conducted a compression test on deformable cell membrane model using the neo-Hookean membrane model, Mooney-Rivlin cell membrane model and Yeoh 's model. It was reported that the Mooney-Rivlin model could describe the behavior of cell deformation the closest to the experimental results (Rachik et al., 2006).

1.3 Problem Statement

The effect of varying P-selectin density on deformable leukocytes has not been investigated significantly by using computational tools. We have used the existing model (Jadhav et al.,2005, Pawar et al.,2008 and Balsara et al. 2015) that simulates the motion of elastic capsule decorated with PSGL-1 molecules (representative of a deformable PMN) rolling on a planar substrate coated with varying density of P-slectin molecules. We can simulate through a Monte Carlo process bond formation based on the proximity of ligands to the receptors present on the surface using the Bell model (Bell, 1978). The study presented in this thesis focuses on analyzing the effects of changing the receptor density on the motion and physical behavior of elastic capsule.

Additionally, the effect of varying the first-order rate constant for dissociation of the receptor-ligand bond , k_{off} is observed on the number of bonds formed and the bond lifetime at a range of P-selectin density from 30 molecules per μm^2 to 150 molecules per μm^2 at a higher shear rate of 400 s^{-1} .

1.4 Research Scope

With an interest to simulate the PSGL-1 mediated PMN rolling, adhering to the surface patterned with P-selectin in a shear flow, this thesis addresses the effect of uniform patterning of P-selectin on the cell rolling, cell-substrate contact area and receptor-ligand binding. Through an algorithm developed by our lab (Jadhav et al.2005, Pawar et al. 2008, Balsara et al. 2015), Immersed boundary method was used to simulate the motion of an elastic capsule (representative of a PMN), on a plane (representative of an endothelial cell), in a linear shear field. The spatial order of accuracy of the Immersed boundary method was second order globally, and first order near the interface (Pawar 2008). The numerical method employed is semi-implicit and first order in time. The Finite element method was used with a Mooney Rivlin strain energy density function to calculate the nodal forces. The stochastic nature of bond formation and breakage was simulated using the Monte Carlo method governed by binding kinetics based on Bell model (Bell, 1978) since the Bell model has been observed to accurately describe the receptor-ligand bond formation and breakage (Chen and Springer 2001; Krasik and Hammer 2004). The cell surface was coated with rigid microvilli and PSGL-1 were mounted on the tip of these microvilli. The Immersed Boundary Method was originally developed by Peskin and McQueen, 1989 to simulate the blood flow in the heart, since then it has found multiple applications in simulating the flow in biological systems (Eggleton and Popel, 1998). The stochastic binding kinetics algorithm has been successfully modified to account for the change in cell shape in order to study the cell-substrate contact area and cell rolling velocity. The fluid grid was discretized for 64 X 64 X 128 nodes with 128 nodal discretizations being in the direction of flow. The cell membrane was discretized into 10,240 triangular element nodes. In order to make the model computationally cost-effective, PMN sedimentation was neglected. Thus, the simulation was initialized with the cell placed 75 nm above the substrate. With that view, the primary goal of this thesis is to study the effect of uniform patterning of the substrate on the cell rolling and adhesion behavior so as to provide a prediction for in vivo experiments involving similar approach.

All the observations are for a capsule having a membrane elasticity, $E_h = 0.3$ dynes/cm, with a raidius of 3.75 µm, suspended in a fluid with a viscosity of 0.8 cP. The Reynolds number for these simulations is 1.76×10^{-3} to 7.03×10^{-3} which is <<1 and the capillary number is in the range from 1×10^{-3} to 4×10^{-3} . The microvilli are considered to be rigid protrusions on the elastic capsule and

the PSGL- molecules are considered to be mounted on the tips of microvilli. The planar surface is uniformaly patterned while varying the P-selectin density.

The primary focus of this investigation was to access or study the effect of varying the surface density of P-selectin molecules on th physical response or characteristics of PMN rolling Several physical factors are investigated, including the capsule-surface contact area, the capsule deformation, the receptor-ligand bond lifetime, the number of receptor-ligand bonds formed to list a few. Investigating the effect of changing the P-selectin density on the physical behavior of an elastic capsule is important because the The computational tools can be applied to the design of in vitro microchannels that employ variation in the surface density of P-selectin molecules to achieve a biotechnology objective.

Chapter 2: Computational model

2.1 Overview

A leukocyte is modeled as a spherical capsule having an elastic membrane, with an ability to deform in response to hydrodynamic and other forces.. The magnitude of the elasticity of this capsule is based on the leukocyte (PMN) deformation observed in vivo for the intensity of shear stress typical in venous circulaton (Turitto,1982) (Damiano et al., 1996; Smith et al., 2002) and is 0.3 dyn/cm and is suspended in a fluid with viscosity of 0.8 cP. This elastic capsule has a diameter of 7.5 µm (Tandon and Diamond, 1998). The capillary number measuring the ratio of the external viscous forces to the interfacial forces is given by $Ca = \mu GR/\gamma_{eq}$ where the interfacial tension is γ_{eq} , is 1×10^{-3} to 4×10^{-3} . The Reynolds number for these simulations is $1.76 \times 10\text{-}3$ to $7.03 \times 10\text{-}3$ which is $\ll 1$. The elastic capsule has an ability to bind with a surface coated with rigid microvilli. The microvilli play an important roll in binding with the planar surface coated with P-selectin. The computational domain entails a capsule subjected to shear flow, flowing between two parallel plates, where the bottom plate is coated with P-selectin molecules for binding. A no-slip boundary condition is imposed between the capsule and the plates. This model is simulated by combining the: (1) The immersed boundary method to solve the Navier Stokes equation for the motion of an elastic capsule near a planar surface in a linear shear flow field (Eggleton and Popel 1998; Jadhav et al. 2005); (2) The finite element method to solve the a Mooney–Rivlin constitutive equation (Balsara et. al., 2015) used to model the elastic membrane; and (3) The Monte Carlo method for simulating the formation and breakage of receptor-ligand bonds with kinetic rate constants based on the Bell model (Bell 1978).

2.2 Immersed boundary method:

Fluid dynamics problems, defined by differential equations could be simulated by using two different approaches. These approaches are grid topology and conformity with the domain boundaries. The first approach considers the grids which fall onto the boundaries of the computational domain. The second approach considers only the Cartesian topology throughout the domain irrespective of the grid conforming to the boundaries of the domain. The second approach is known as 'Immersed boundary method'

The Immersed boundary method was first developed by Charles Peskin (C.S. Peskin and D.M. McQueen, 1989) to study the fluid-structure interaction of the heart valve systems assuming a very low Reynolds number. It is useful to study complex stationary or moving bodies, with or without moving boundaries. The need of establishing a body-conformal grid at each time step is eliminated. Thus, the solution procedure is significantly simplified. The issues involving grid interpolation and maintaining the grid quality is eliminated.

 In the following work, an elastic capsule filled with Newtonian fluid is considered using the Immersed Boundary method. This method uses both Eulerian and Lagrangian variables. In this paper, the Eulerian variables are defined on a fixed Cartesian grid and the Lagrangian variables are defined on a free moving curvilinear grid. The curvilinear grid can move through the fixed Cartesian grid without being forced to adapt to it with regards to any parameter at all (Peskin 1989).

In this paper, IBM (Immersed Boundary Method) is applied to model a 3D elastic capsule containing Newtonian fluid in the inside and the outside of the capsule. The governing equations for this type of flow can be expressed by the following continuity (2.2.1) and Navier-Stokes equation (2.2.2).

$$\nabla \cdot u \ (x, \ t) = 0 \tag{2.2.1}$$

$$\rho \, \frac{\partial u(x,t)}{\partial t} + \rho u \ (x, \ t). \ \nabla u \ (x, \ t) = -\nabla p \ (x, \ t) + \mu \ \nabla^2 u \ (x, \ t) + F \ (x, \ t) \tag{2.2.2}$$

where, ρ is the density and μ is the viscosity of the fluid, p(x, t) and u(x, t) is the pressure and velocity discretized at each fluid grid notes where x (x, y, z) is the fluid grid node and F (x, t) is

the total external force acting on each fluid grid nodes. This force arises due to the adhesion of the capsule with the surface. Let us consider the Eulerian cartesian fluid grid is x(x, y, z) and the Lagrangian triangular finite element grid be X(X, Y, Z) (Eggleton and Popel, 1998, Pawar et al, 2008, Konstantopoulos et al, 1998)to record the deformation (Pawar 2008). With the start of each time step t, it is empirical to calculate the restoring forces f(X, t) at the immersed boundary nodes arising due to the deformation of the elastic capsule and from the receptor-ligand bond formation where X (q, r, s) denotes the local curvilinear coordinates (Jadhav 2005).

Also, because the Reynolds number for the fluid flow under consideration is very low Re << 1; ignoring the convective terms yield the following equation:

$$\rho \frac{\partial u(x,t)}{\partial t} = -\nabla p \ (x, t) + \mu \ \nabla^2 u \ (x, t) + F \ (x, t) \qquad (2.2.3)$$

The communication between the fluid and the immersed boundary is linked through the spreading of the singular force from the Lagrangian grid to the Cartesian grid and the interpolation of velocity from the Cartesian grid to the Lagrangian grid is bridged by using Dirac delta function. The total external force which acted on each fluid grid nodes, F (x, t), was interpolated from the force field that acts on the immersed boundary nodes, f (X, t), denoted in the local curvilinear coordinate by X (q, r, s). The interpolation of the total external force is performed by a Dirac delta function,

Thus, the total external force F (x, t) can be expressed as (2.2.4)

$$F(x, t) = \int f(X, t) \ \delta(x - X) \ dr \ ds \qquad (2.2.4)$$

where $f(X, t)$ was the restoring forces calculated at the immersed boundary nodes arising due to the displacement of capsule nodes and the stationary plane as well as those due to the adhesion of molecule to the surface and receptor-ligand bond formation. Since $\delta(x)$ is a three dimensional Dirac delta function, it is (Lai and Peskin 2000).

$$\delta(x) = \ \delta(x_1) \ \delta(x_2) \ \delta(x_3) \qquad (2.2.5)$$

The immersed boundary force $f(X, t)$ was computed from the local curvilinear boundary configuration with the coordinates X (q, r, s) and discrete delta function was used to translate the force to fluid

$$\delta_h \ (x) = \ d_h(x) \ d_h \ (y) \ d_h(z) \qquad (2.2.6)$$

where d$_h$ was the 1-D discrete Dirac delta (Lai and Peskin,2000)

$$d_h(r) = \begin{cases} \dfrac{3-\frac{2|r|}{h}+\sqrt{1+\frac{4|r|}{h}-\frac{4|r|}{h^2}}}{8h} & if \ |r| \ \leq h \\ \dfrac{5-\frac{2|r|}{h}-\sqrt{-7+\frac{12|r|}{h}-\frac{4|r|}{h^2}}}{8h} & if \ h \ \leq \ |r| \ \leq 2h \\ 0 & if \ otherwise \end{cases}$$ (2.2.7)

where, h was the uniform mesh width.

Here, the Discrete Dirac delta function is chosen to be continuous and to be a singular source to the grid points in vicinity (Zhilin Li 2003).

Since we are using the continuous formulation approach for the Dirac delta function, the total external force $F(x,t)$ is typically an integral over a local $f(X)$. Corresponding to this we can express the approximate Dirac delta function as (Peskin 2003):

$$F(x,t) = \sum_{q,s} f(X,t).\delta_h(x-X) \ \Delta q \ \Delta s$$ (2.2.8)

A no-slip boundary condition is considered and is expressed by assuming the cell nodes move with the same velocity as the velocity of the nearby fluid nodes (Eggleton, 2012).

$$U(x,t) = \int_{\Omega} u(X,t) \ \delta(x-X)dX$$ (2.2.9)

Which is approximated as,

$$U(x,t) = \sum_{q,s} u(X,t).\delta_h(x,X) \ \Delta q \ \Delta s$$ (2.2.10)

At the end of each fractional time step, the position of the cell nodes are updated using the relationship (Szatmary 2012),

$$X^{n+1} = X^n + \Delta t \ U^{n+1}(X^n,t)$$ (2.2.11)

The above method   is considered as a mathematical formulation and as a numerical scheme. However, it does not include any discussion about the type of fluid solver used (Szatmary 2012). The continuity equation and the Navier Stokes equation is discretized in space and time. Finite difference method is used to represent it on a 3D uniform cartesian grid. The velocity and pressure is accounted at each fluid grid nodes .

Then introduced by Chorin and Temam is used to solve Navier-Stokes equation. This method is also called as fractional-step projection method. Chorin's projection method is a great tool to decouple the fluid velocity and pressure fields at each fluid grid nodes.

Schematic for the Immersed boundary method:

At each time step:

```
┌────────────────────────────────────┐
│     Compute boundary force f (X,t)  │
└────────────────────────────────────┘
                 │
                 ▼
┌────────────────────────────────────┐
│  Apply boundary force to Total      │
│          external force             │
└────────────────────────────────────┘
                 │
                 ▼
┌────────────────────────────────────┐
│  Implement no slip boundary condition│
└────────────────────────────────────┘
                 │
                 ▼
┌────────────────────────────────────┐
│    Calculate velocity for fluid grid │
└────────────────────────────────────┘
                 │
                 ▼
┌────────────────────────────────────┐
│    Calculate membrane node velocity │
└────────────────────────────────────┘
                 │
                 ▼
┌────────────────────────────────────┐
│    Update the positon of membrane   │
└────────────────────────────────────┘
```
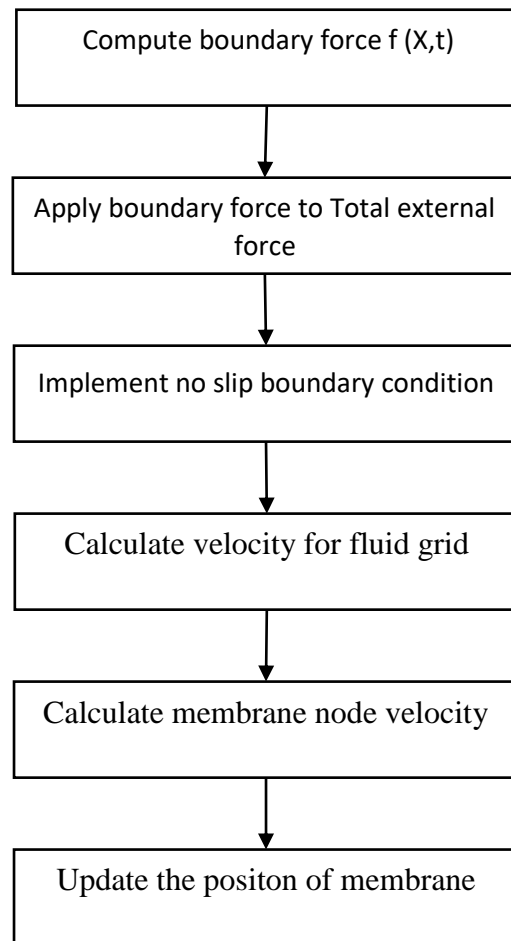
2.2.1 Chorin's Projection Method:

We first compute the intermediate velocity u^* using momentum equation while ignoring the pressure gradient term and incompressibility.

$$\frac{u^*-u^n}{\Delta t} = -(u^n.\nabla)u^n + v\nabla^2 u^n \tag{2.2.12}$$

where u^n is the velocity at n^{th} time step. Computing an intermediate velocity u^n while ignoring the pressure gradient term and incompressibility. Then solving the time discretized equation. Once we find F(x,t), the total external force acting on each fluid grid nodes, we use this method to solve the unsteady Stokes equation. Solving for initial velocity:

$$u^{n+1,0} = u^n + \frac{\Delta t}{\rho} F^n \tag{2.2.13}$$

Solving for intermediate velocity in every coordinate direction:

$$\rho\left[\frac{u^{n+1,1}-u^{n+1,0}}{\Delta t}\right] = \mu D_1^+ D_1^- u^{n+1,1} \tag{2.2.14}$$

$$\rho\left[\frac{u^{n+1,2}-u^{n+1,1}}{\Delta t}\right] = \mu D_2^+ D_2^- u^{n+1,2} \tag{2.2.15}$$

$$\rho\left[\frac{u^{n+1,3}-u^{n+1,2}}{\Delta t}\right] = \mu D_3^+ D_3^- u^{n+1,3} \tag{2.2.16}$$

where D_α^- and D_α^+ are the backward and forward difference operators for differentiating u.

$$(D_\alpha^- u)(x) = \frac{u(x)-u(x+he_\alpha)}{h} \tag{2.2.17}$$

$$(D_\alpha^+ u)(x) = \frac{u(x+he_\alpha)-u(x)}{h} \tag{2.2.18}$$

Taking the following pressure term in consideration and solving for p^{n+1} and u^{n+1}:

$$\rho \left(\frac{u^{n+1} - u^{n+1,3}}{\Delta t} \right) + D \, p^{n+1} = 0 \tag{2.2.19}$$

$$D \cdot u^{n+1} = 0 \tag{2.2.20}$$

where D is the discrete divergence operator.

In 3 dimensions, D has the following form (Rosar and Peskin 2001):

$$(D.u)(x) = \sum_{x'} \left[u_1(x_1', x_2', x_3') \gamma(x_1 - x_1') \omega(x_2 - x_2') \omega(x_3 - x_3') + \right.$$

$$u_2(x_1', x_2', x_3') \gamma(x_2 - x_2') \omega(x_1 - x_1') \omega(x_3 - x_3') +$$

$$\left. u_3(x_1', x_2', x_3') \gamma(x_3 - x_3') \omega(x_1 - x_1') \omega(x_2 - x_2') \right] \tag{2.2.21}$$

where,

$$\gamma(x) = \eta(x - X) \Big|_{X = -\frac{h}{2}}^{X = \frac{h}{2}} \tag{2.2.22}$$

$$\omega(x) = \int_{-\frac{h}{2}}^{\frac{h}{2}} \eta(x - X) \, dX \tag{2.2.23}$$

where $\eta(x)$ was defined as:

$$\eta(x) = \begin{cases} \frac{1}{4h} \left(1 + \cos\left(\frac{\pi x}{2h}\right) \right) & |x| \leq 2h \\ 0 & |x| > 2h \end{cases} \tag{2.2.24}$$

The above discrete divergence operator can also be defined as:

$$D.u = D_1 \cdot u_1 + D_2 \cdot u_2 + D_3 \cdot u_3 \tag{2.2.25}$$

where the operators D_1, D_2, D_3 were of the form

$$(D_1 \emptyset)(x_1, x_2, x_3) = \sum_{(x_1', x_2', x_3')} u_1(x_1', x_2', x_3') \, \gamma(x_1 - x_1') \, \omega(x_2 - x_2') \omega(x_3 - x_3') \tag{2.2.26}$$

$$(D_2\emptyset)(x_1, x_2, x_3) = \sum_{(x_1', x_2', x_3')} u_2(x_1', x_2', x_3') \, \gamma(x_2 - x_2') \, \omega \, (x_1 - x_1')\omega \, (x_3 - x_3') \quad (2.2.27)$$

$$(D_3\emptyset)(x_1, x_2, x_3) = \sum_{(x_1', x_2', x_3')} u_3(x_1', x_2', x_3') \, \gamma(x_3 - x_3') \, \omega \, (x_1 - x_1')\omega \, (x_2 - x_2') \quad (2.2.28)$$

these discrete divergence operators can also be used for a discrete gradient. Thus we get,

$$D\emptyset(x) = (D_1\emptyset(x), D_2\emptyset(x), D_3\emptyset(x)) \qquad\qquad (2.2.29)$$

The discretized continuity equation (2.2.20), will be used to simplify the pressure step in eqation (2.2.19) as follows:

However, since divergence of u^{n+1} is equal to zero from equation (20), equation (2.30) reduces to:

$$\left(\frac{\rho D \cdot u^{n+3}}{\Delta t}\right) = D \cdot D \, p^{n+1} \qquad\qquad (2.2.30)$$

2.3 Finite Element Method:
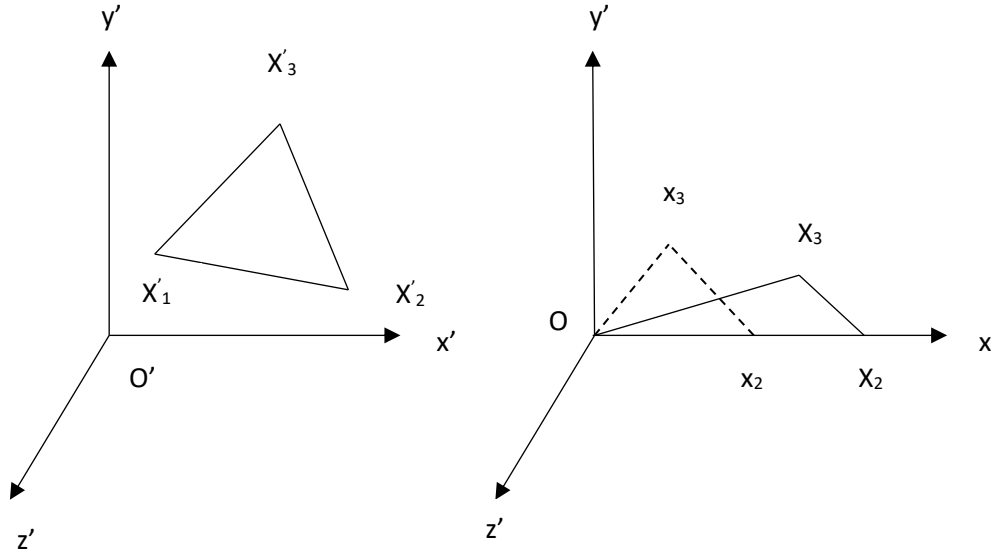
Figure 2.3: (a) An arbitrary element in a 3-D space

(b) The element is transformed into 2-D space. The dashed lines represent undeformed position of the element x_i and the solid triangle represents the deformed element denoted by X_i. Node x_i is the origin O.

The capsule membrane was discretized into a mesh of triangular elements. The mesh was generated in a 3D space and was then transformed into a 2D space. Let the undeformed coordinate system be (x, y). Once the rolling motion begins, the capsule starts deforming. The deformation implies that the node position has to be updated, this is done by using equation (2.2.11). The deformed coordinate system was denoted by (X,Y). This leads us to compute the nodal displacements using the equation:

$$u_i = X_i - x_i \tag{2.3.1}$$

$v_i = Y_i - y_i$ (2.3.2)

where i=1,2,3 correspond to nodal points on the vertices of the triangular element.

The displcement fields u and v are linear functions of position. These linear functions can be expressed as:

$$u = N_i u_i$$ (2.3.3)

$$v = N_i v_i$$ (2.3.4)

where N_i was the shape function defined as $N_i (x_i, y_i) = 1$ when $i = j$ and $N_i (x_i, y_i) = 0$ when $i \neq j$.

The shape function is defined as

$$N_i = \frac{(a_i x + b_i y + c_i)}{L_i}$$ (2.3.5)

where,

$$a_i = y_i - y_k \; ; b_i = x_k - x_j; \; c_i = x_j y_k - x_k y_j$$ (2.3.6)

$L_i = a_i x_i + b_i y_i + c_i$ (2.3.7)

The displacement gradients are expressed as:

$$\frac{\partial u}{\partial x} = u \cdot A \; , \frac{\partial u}{\partial y} = u \cdot B, \frac{\partial v}{\partial x} = v \cdot A, \frac{\partial v}{\partial y} = v \cdot B$$ (2.3.8)

where $u = [u_i]$, $v = [v_i]$, $A = [a_i / L_i]$, and $B = [b_i / L_i]$.

A deformation gradient tensor is used to relate the deformed and undeformed nodal positions such as dX = Fdx, where F was the deformation gradient tensor given by:

$$F = \begin{bmatrix} 1 + \left(\frac{\partial u}{\partial x}\right) & \left(\frac{\partial u}{\partial y}\right) \\ \left(\frac{\partial v}{\partial x}\right) & 1 + \left(\frac{\partial v}{\partial y}\right) \end{bmatrix} \qquad (2.3.9)$$

The above equation is used to calculate the right Cauchy-Green deformation tensor,

$C = F^T F$. Thus we get:

$$C_{11} = (1 + \frac{\partial u}{\partial x})^2 + \left(\frac{\partial v}{\partial x}\right)^2 ,$$

$$C_{22} = (1 + \frac{\partial v}{\partial y})^2 + \left(\frac{\partial u}{\partial y}\right)^2,$$

$$C_{12} = (1 + \frac{\partial u}{\partial x}) \left(\frac{\partial u}{\partial y}\right) + (1 + \frac{\partial v}{\partial y}) \left(\frac{\partial v}{\partial x}\right) \qquad (2.3.10)$$

Substituting equation 2.3.8 in 2.3.10 we get:

$$C_{11} = 1 + 2u \cdot A + (u \cdot A)^2 + (v \cdot A)^2$$

$$C_{22} = 1 + 2v \cdot B + (u \cdot B)^2 + (v \cdot B)^2$$

$$C_{12} = (1 + v \cdot B)v \cdot A + (1 + u \cdot A)u \cdot B \qquad (2.3.11)$$

The derivative of each components of the right Cauchy-Green strain tensor is calculated with respect to each component of u and v to formulate the principal stretch ratios as follows:

$$\lambda_1 = \frac{1}{2}[\, C_{11} + C_{22} + \sqrt{(C_{11} - C_{22})^2 + 4C_{12}^2}\,]$$

$$\lambda_2 = \frac{1}{2}[\, C_{11} + C_{22} - \sqrt{(C_{11} - C_{22})^2 + 4C_{12}^2}\,] \qquad (2.3.12)$$

Using Principal of virtual work, a relationship was derived between the nodal displacements and nodal forces. This is expressed as (Charrier et al., 1989):

$$\delta \text{ W}_\text{e} = u^T F_x + v^T F_y \tag{2.2.13}$$

where $\delta \text{ W}_\text{e}$ was the actual external work done and F_x and F_y are the nodal forces experienced

in the x and y direction for the current configuration of the system. Since the stretch ratios were

constants, the above equation can be also represented as:

$$\delta \text{ W}_\text{e} = \text{V}_\text{o} \, \delta \text{ W} \tag{2.2.14}$$

where W was the strain energy density, V was the volume of the triangular element. For the

hyperelastic material underconsideration, for the capsule to be incompressible, $\lambda_1 \, \lambda_2 \, \lambda_3 = 1$

should be satisfied. Thus, the first order variation of strain energy density function is given by

$$\delta \text{ W} = u^T \left[\frac{\partial W}{\partial \lambda_k} \frac{\partial \lambda_k}{\partial u_i} \right] + v^T \left[\frac{\partial W}{\partial \lambda_k} \frac{\partial \lambda_k}{\partial v_i} \right] \tag{2.3.15}$$

Substuting equation 2.3.13 and 2.3.15 in equation 2.3.14, we can determine the force experienced

by the node as:

$$F_{xi} = \text{V}_0 \left[\frac{\partial W}{\partial \lambda_k} \frac{\partial \lambda_k}{\partial u_i} \right] \text{ and } F_{yi} = \text{V}_0 \left[\frac{\partial W}{\partial \lambda_k} \frac{\partial \lambda_k}{\partial v_i} \right] \tag{2.3.16}$$

Knowing that the hyperelastic membrane is assumed to have a spherical and stress-free shape, the

nodal forces can be calculated from the nodal displacements of an element by employing the

appropriate strain energy density function. For the current study, the strain energy density function

in form of Mooney-Rivlin membrane was used:

$$\text{W} = \frac{Eh}{6} [(\lambda_1^2 + \lambda_2^2 + \lambda_1^{-2} \lambda_2^{-2} - 3) + \Gamma(\lambda_1^2 \lambda_2^2 + \lambda_1^{-2} + \lambda_2^{-2} - 3] \tag{2.3.17}$$

where E is Youngs modulus for the elastic material, h is the membrane thickness and in order to

study the effect of degree of strain stiffening, dimensionless constant Γ is considered equal to zero

in equation (26), this defines the strain energy density function for neo-Hookean membrane. The

neo-Hookean membrane is assumed to be initially isotropic and incompressible. The principal of virtual work is used to derive the relationship between nodal displacement and nodal forces. These in-plane forces are computed at the vertices of each triangular element using finite difference procedure outlined in Charrier et al. (1989) and Eggleton and Popel (1998).

2.4 Monte Carlo simulation for Receptor-Ligand binding:

The cell either advances forward or ceases to move in order to transmigrate based on its binding kinetics. The simulation of binding kinetics entails the bond formation and/or bond dissociation of the capsule rolling on the selectin coated surface. These processes are defined by the bond formation rate k_f and bond dissociation rate k_r . Here, the receptor-ligand interaction is defined by employing the Bell model (Bell 1978). According to this model, the forward and reverse rate is defined by:

$$k_f = k_f^0 \exp\left[\frac{\sigma_b |L_b - L_{b0}|\left(x_\beta - \frac{1}{2}|L_b - L_{b0}|\right)}{k_B T}\right]$$
(2.4.1)

$$k_r = k_r^0 \exp\left[\frac{(x_\beta F)}{k_B T}\right]$$
(2.4.2)

where k_f^0 and k_r^0 are the forward and reverse rate constants at the equilibrium

distance L_{b0}; $k_B T$ is the thermal energy; σ_b is the spring constant in the bond state; and L_b was the length of the possible new bond, x_β is the reactive compliance and F is the force acting on the bond.

The bond decay rate without rebinding is given by the equation (Eggleton et. al.,2012).

$$\frac{dN}{dt} = -Nk_r$$
(2.4.3)

where N(t) isthe number of bonds and dN/dt is the time derivative of Number of bonds formed at any time t.

Equating equations 2.34 and Equation 2.35 gives

$$k_r^0 = \frac{-\frac{1}{N(t)}\frac{dN}{dt}}{\exp\left(\frac{x_\beta F}{k_\beta T}\right)}$$
(2.4.4)

The force acting on the bond can be expressed as:

$$F = \sigma_b (L_b - L_{b0}) \qquad (2.4.5)$$

Bond formation and dissociation is a stochastic process, thus Monte- Carlo simulation is used to predict its probability to bind or rupture. The probability that the receptor will bind, P_f, or an existing bond will rupture P_r, for a given time interval Δt, is given by Hammer and Apte (1992):

$$P_f = 1 - \exp(-k_{on} \Delta t) \qquad (2.4.6)$$

$$P_r = 1 - \exp(-k_r \Delta t) \qquad (2.4.7)$$

where $k_{on} = k_f A_L (n_L - n_B)$. A_L is the surface area on selectin-coated plane accessible to each PSGL-1, whereas $(n_L - n_B)$ is the density of unbound ligand. The bond formation and/or rupture is determined by comparing the above mentioned probabilities with two random numbers P_{ran1} and P_{ran2}, which are between 0 and 1. If P_f is greater than P_{ran1}, then the bond has formed, whereas P_r greater than P_{ran2} suggests that the bond has ruptured. At every time step, the number of bonds formed and ruptured are recorded. A time step of 10^{-6} is used to simulate the cell rolling for a period of 1s. In addition, the microvillus is modelled as solid, rigid cylinders that does not deform under force. It is important to note that the surface roughness caused due to these rigid microvilli are not accounted by the IBM while performing the simulation to capture the motion of the cell.

Chapter 3 Calibration of model with published data:

In this chapter, the results obtained from simulations are validated with the published data of (Balsara et al., 2015), who used a Mooney-Rivlin constituitive relationship for the capsule membrane where the value of Γ was varied from zero to one, and the P-selectin density was kept constant. In order to validate, the model parameters were defined to mimic the model as described in Balsara et al. 2015. The parameter values were as described in Table 3.1.

Parameters	Definition	Value	Reference
R	Capsule radius	3.75μm	(Tandon and Diamond, 1998)
Lm0	Equilibrium length of microvilus	0.35 μm	(Shao et al., 1998)
N_{mv}	No. microvilli/cell	252	(Chen and Springer, 1999)
NL_{mv}	No. PSGL-1 mol/microvillus	50	(Moore et al., 1991)
NL	No. PSGL-1 mol/cell	15000	(Moore et al., 1991)
x_{β}	Reactive compliance	$0.3\dot{A}$	(Caputo and Hammer, 2005)
L_{b0}	Equilibrium bond length	0.1 μm	(Fritz et al., 1998)
k_r^0	Unstresed off rate	$1\ s^{-1}$	(Mehta et al., 1998)
k_f^0	Unstresed on rate	$1\ s^{-1}$	(Mehta et al., 1998)
σ_b	Bond spring constant	1 dyn/cm	(Dembo, 1994)
σ_{ts}	Transition state spring constant	0.99 dyn/cm	(Dembo, 1994)
E_h	Membrane stiffness	0.3 dyn/cm	(Jadhav et al., 2005)
Γ	Dimensionless parameter	0 - 1.0	(Hiren et al., 2015)
γ	Shear rate	$100 – 400\ s^{-1}$	(Hiren et al., 2015)
μ	Fluid viscosity	0.8 cP	
NR	P-selectin(receptor) site density	$30 – 150/\mu m^2$	
ρ	Fluid density	1 g/cc	
T	Temperature	310 K	

A comparison between bond lifetime of cell membrane compared with the data presented in Balsara et al. (2015) is shown in Figure 4.1. The resuts vary by <6% with the previously published data, and this is discrepancy attributed to to the stochastic nature of the receptor-ligand binding kinetics.
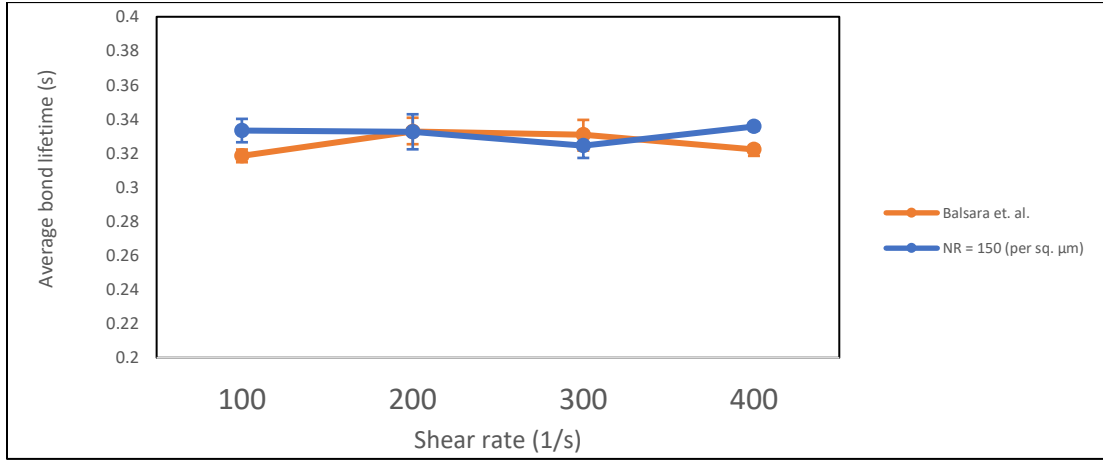

Figure 3.1: The bond lifetime for the receptor-ligand bonds is computed and is shown for varying shear rate. The bond lifetime computed from the present simulation (orange line) was compared with the published data (blue line).

The bond lifetime for a capsule was computed at shear rates varying from 100 s^{-1} to 400 s^{-1}. These results were computed for the cell's lifetime of 1s and was then compared to the published results (Balsara et al., 2015) and are displayed in Figure 4.1. The simultions were conducted multiple times with the parameters listed in Table 4.1 due to the stochasitc nature of receptor-ligand bond formation.

By comparing the results for bond lifetime, one can conclude that the results are within the margin of error; thus the results are reliable. Also, we have to note that there will always be a certain amount of discrepancy between the published data and the results generated by our current study due to the stochasitc nature of bond formation. The bonds can never be formed at the exact same locations and so there is a slight devation in the data generated in this study and the published data (Balsara et al., 2015).

Chapter 4: Results and Discussion

4.1 Capsule membrane deformabiltiy in a shear flow field:

4.1 Effect of NR on Average number of bonds formed in linear shear flow:

This study encompasses the effects caused on the cell binding kinetics due to varying the physical parameter P-selectin density coated on the substrate in the shear flow. As the substrate was augmented with the P-selectin molecules ranging from 30 molecules/μm^2 to 150 molecules/μm^2, an increase in the bond formation was observed.

It is interesting to see that the number of receptor-ligand bonds formed increased as the shear rate was increased from 100 s^{-1} to 400 s^{-1}. At a lower shear rate of 100 s^{-1}, the average bonds formed between the receptor and ligands for the P-selectin site density (hereafter referred to as NR) of 150 molecules/μm^2 was five times greater than the bonds formed when the NR was 30 molecules/μm^2. Thus a drastic increase in the number of bonds formed is observed when the P-selectin density on the substrate is increased.

As observed from the figure 4.1 , the number of bonds formed at a shear rate of 300 s^{-1} is greater as compared to the bonds formed at a shear rate of 400 s^{-1} when the NR is 150 molecules/μm^2, however, the difference is 4% which is not significant considering the stochastic nature of bond formation.

The bond formation and its rupture depends upon the bond formation rate k_f and the rate of bond dissociation. In our study we the receptor-ligand interaction is defined by employing the Bell (Bell, 1978) approach. According to Bell model theory, we have used the equations (2.33) and (2.34) to define the rate of bond formation and rate of bond dissociation. The rate of bond formation and the rate of bond dissociation was then used to determine the probability of bond formation and probability of bond rupture.

The main reason for an increased bond formation at a higher value of shear rate is attributed to an increase in the deformation of capsule as the shear rate increases.This increase in the deformation of capsule leads to an increase in the capsule-substrate contact area. Thus the increased contact area at higher shear rate causes an increase in the number of 'sites' at which the bond formation can take place. In other words, increasing the probability of bond formation. Thus we can say that

an increase in the P-selectin site density, leads to an increase in the number of bonds formed. Also, even though the the number of bonds formed increased as the shear rate increased, the increase was not very pronounced. The shear rate did affect the number of bonds formed, but not in a very striking strong manner.
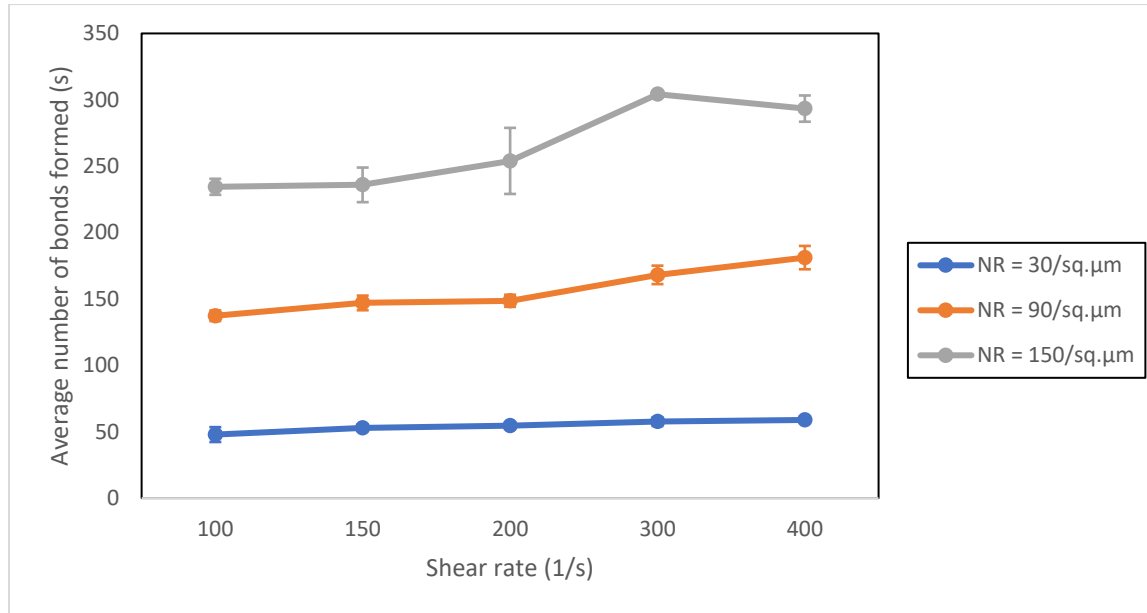
Figure 4.1: Average number of receptor-ligand bonds formed as a function of shear rate for P-selectin site density of 30 molecules per μm^2, 90 molecules per μm^2 and 150 molecules per μm^2
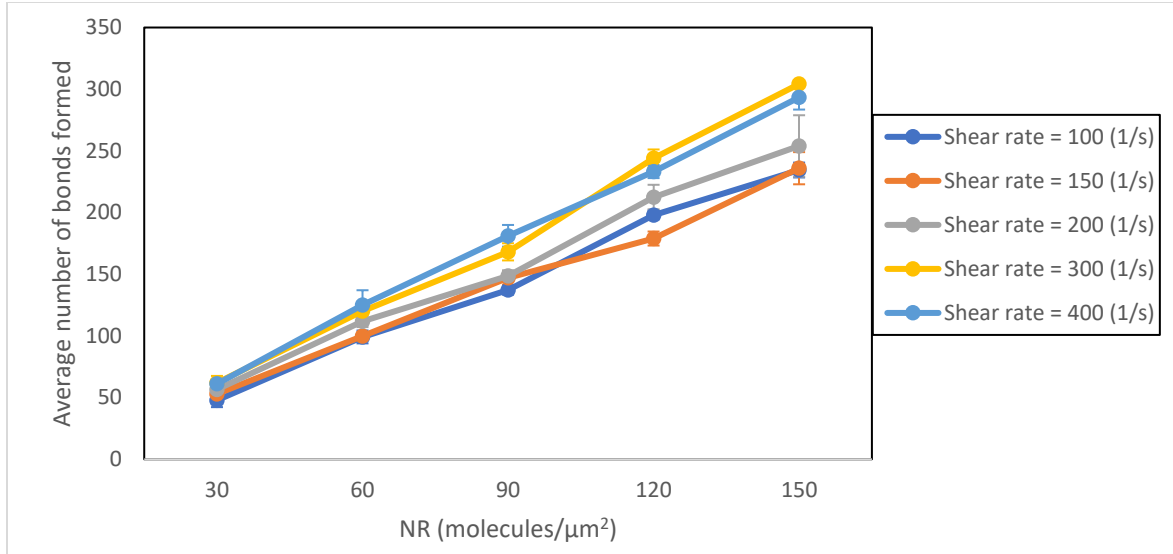
Figure 4.2: Average number of receptor-ligand bonds formed as a function of P-selectin site density computed over a shear rate ranging from 100 to 400 s^{-1} .

4.2 Effect of NR on Total Bond force in linear shear flow:

Figure 4.3: Total receptor-ligand bond force acting on a capsule is calculated over a function of ligand-density from 30 molecules/μm^2 to 150 molecules/μm^2 at shear rates varying from 100 to 400 s^{-1}

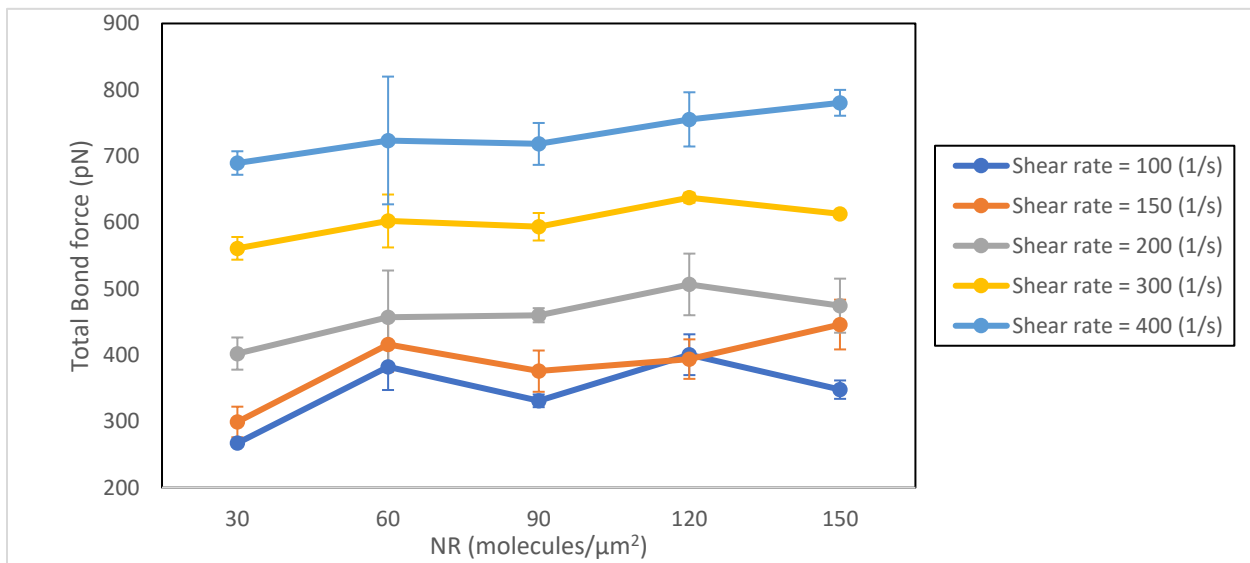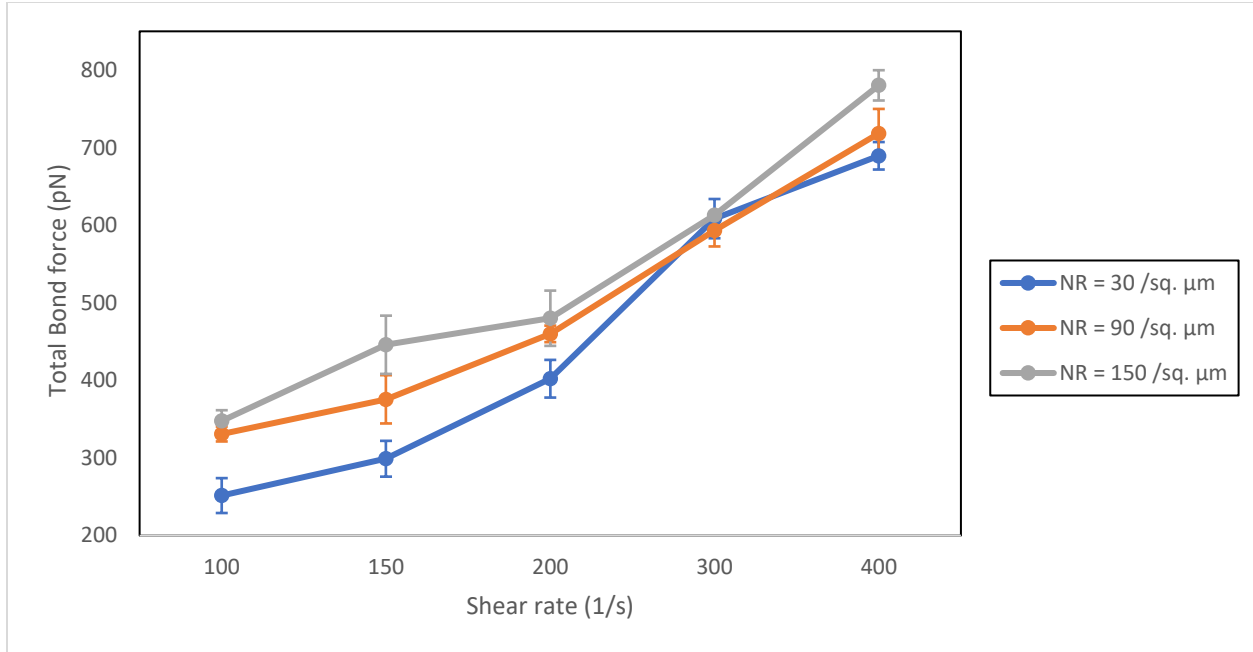Figure 4.4: Total receptor-ligand bond force acting on a capsule is calculated over shear rate ranging from 100 to 400 s^{-1} for P-selectin site density of 30 mo lecules per μm^{-2} , 90 molecules per μm^{-2} and 150 molecules per μm^{-2}

The receptor-ligand bond force is computed while assuming the bond force to be zero when the bond length is less than the equilibrium bond length, this condition ensures that the total bond force is accounted for, only when there is a bond formation. It is observed from figure 4.3 and 4.4 that the total bond force is greater for the cell rolling on a site with higher NR value. On an average, the difference in the total bond force between NR 30 molecules/μm^2 and 150 molecules/μm^2 is 21%. This is observed due to an increased number of bonds formed with an increased NR value. It is also observed that the total receptor-ligand bond force experienced by the capsule at a higher shear rate of 400 s-^{1} is on an average 81% higher than the bond force experienced by the capsule at a lower shear rate of 100 s-^{1} . The capsule experienced the highest difference of 93% in the total bond force while rolling on a substrate with an NR 30 molecules/μm^2. This is attributed to the fact that the bond force is greater on the individual bonds when the bond formation is less such as in case of a capsule rolling on a substrate with NR 30 molecules/μm^2 .

4.3 Effect of NR on Bond lifetime in linear shear flow:
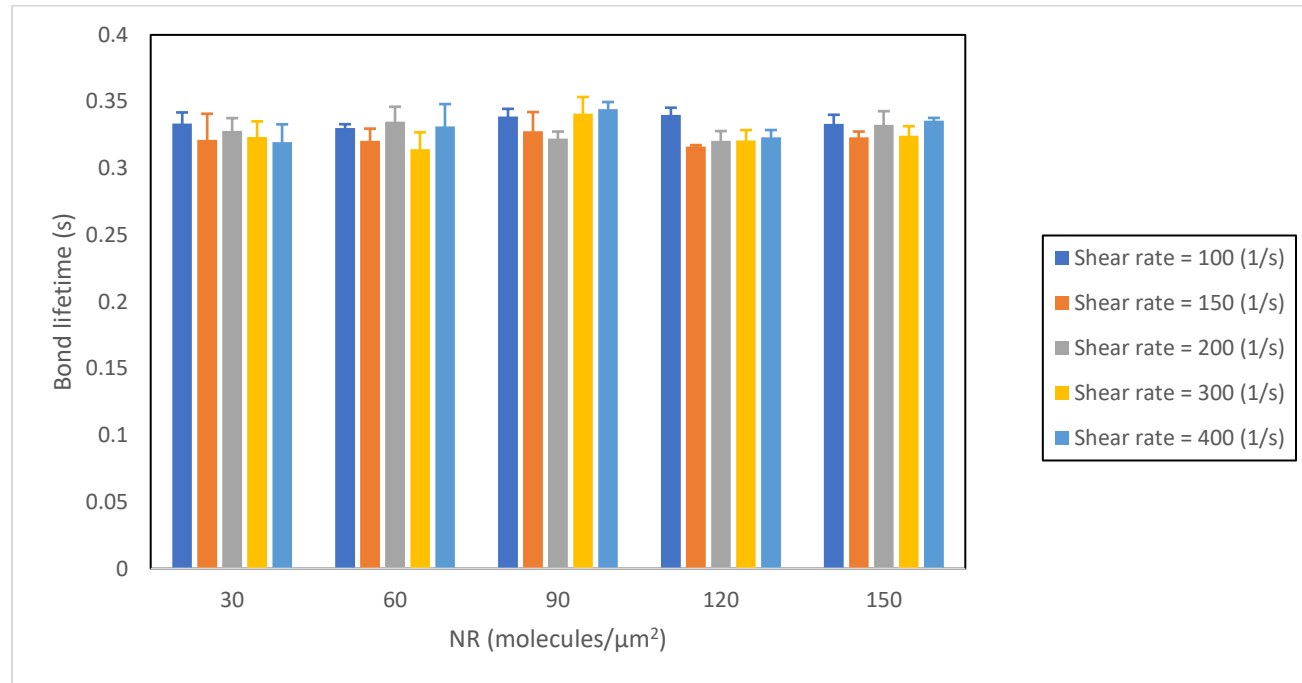
Figure 4.5: The average receptor-ligand bond lifetime during cell rolling on selectin coated substrate was calculated at a shear rate of 100 to 400 s^{-1} for P-selectin density (NR) values of 30 molecules/µm^2 ,60 molecules/µm^2 ,90 molecules/µm^2 ,120 molecules/µm^2 ,150 molecules/µm^2.

Figure 4.5 shows the effect of P-selectin density on the lifetime of bond for a simulation time of 1s. As we can observe from the above figure, the bond lifetime is not entirely dependent on the NR value or the shear rate. Thus, it is uncertain to comment about the trend observed for bond lifetime.

4.4 Effect of NR on Average rolling velocity of capsule in linear shear flow:
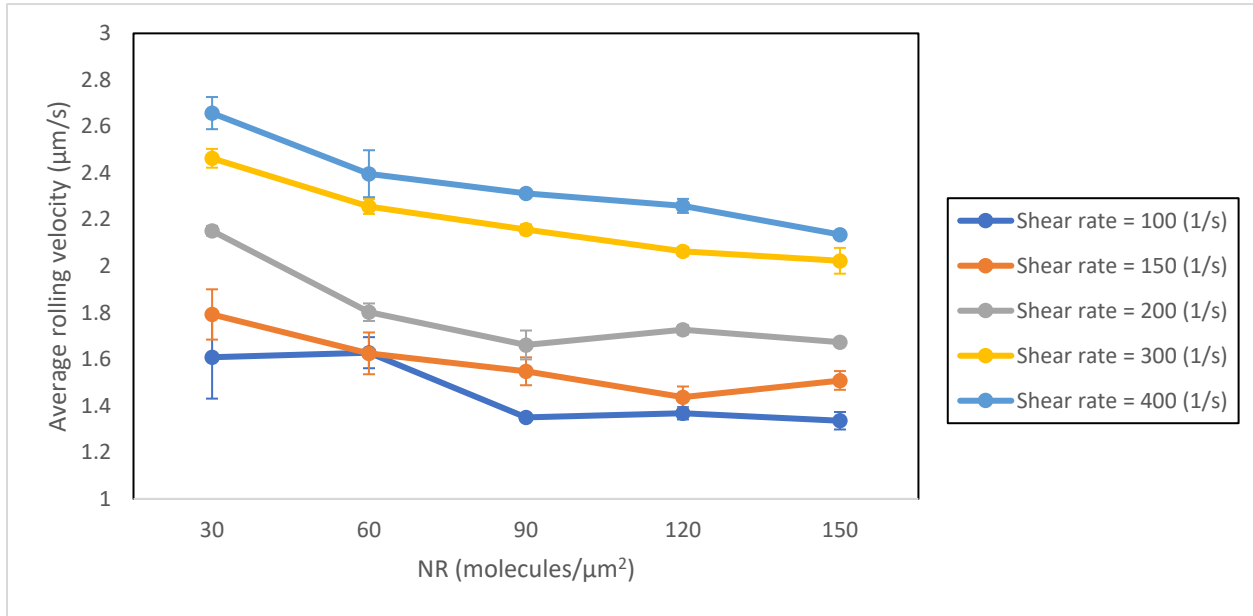
Figure 4.6: The average rolling velocity of the capsule rolling on a substrate with P-selectin density ranging from 30 to 150 molecules/µm^{-2} was recorded for shear rate ranging from 100 to 400 s^{-1} .
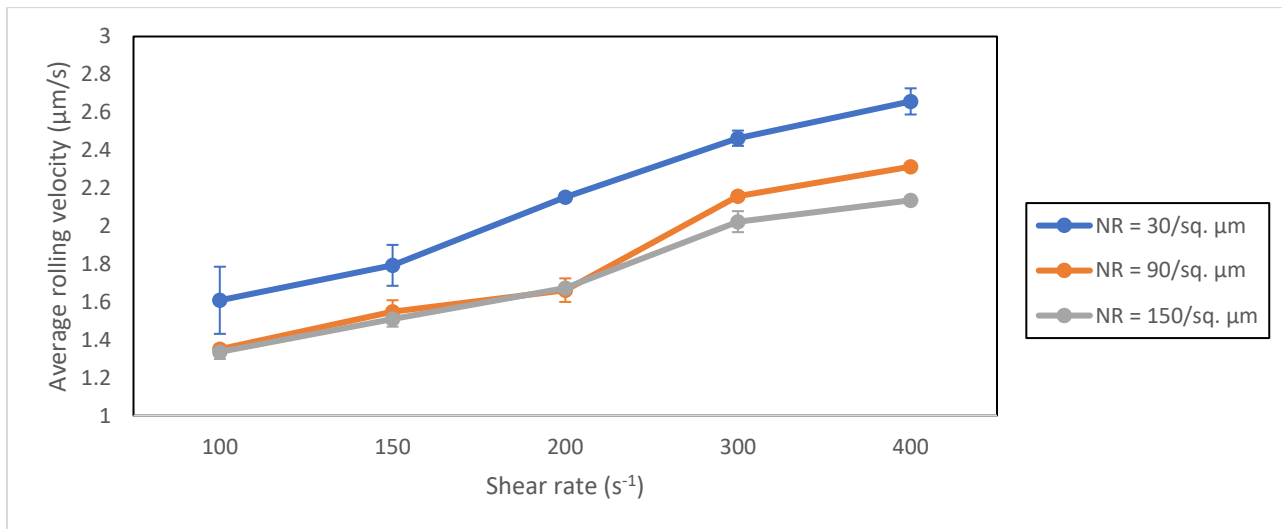
Figure 4.7: The average rolling velocity of the capsule rolling as a function of shear rate from 100 to 400 s^{-1} is computed for a substrate with P-selectin density of 30 molecules/µm^{-2}, 90 molecules/µm^{-2} and 150 molecules/µm^{-2}

The rolling velocity of a capsule on a substrates coated with NR = 30, NR=90 and NR=150 molecules/sq. µm is observed to increase by 49%, N% and 46%, respectively,when the shear rate is increased from 100(units) to 400 (units). A significant increase in the capsule rolling velocity was observed with shear rate, as expected.. The average percent difference between the rolling velocity of a capsule roling on NR=30 molecules/sq. µm and NR=150 molecules/sq. µm at all considered shear rates is calculated to be 20.41%. At NR=30 molecules/sq. µm , the rolling velocity of the capsule increased from approximately 1.6 µm/s to approximately 2.6 µm/s. However, there was only a modest change in the average rolling velocity at higher P-selectin densities NR=range). Since the simulations are stochastic, the similarity of rolling velocities does not necessarily mean that the rolling velocity is always the same. The stochastic simulations lead to different variances in the rolling velocities.

Next, we analyzed the stability of cell while rolling. This was recorded as the variance in the instantaneous velocity. As observed from the figure, it is imporatnt to note that worthy at lower shear rates from 100 s-^{1} to 200 s-^{1} , the rolling stability of the cell was observed to be similar, however at higher shear rates ranging from 200 s-^{1} to 400 s-^{1}, there was a noticeable difference in the stability of the cell rolling on the substrate coated with lower P-selectin site density of 30 µm^{-2} and the rolling of the cell on the substrate with P-selectin density of 150 µm^{-2} . At higher shear rates the percent difference in the variance of instantaneous velocity is 13% which is considerable as compared to the difference at lower shear rates.

 This instability in rolling amongst the capsules rolling on the substrate coated wth less P-selectin density can be attributed to the less number of bonds formed. More number of bonds formation is observed in the cells rolling on the substrate with higher NR values. This means that the rolling velocity is reduced thereby the smoother rolling on the surface. However, besides the slight increase in the variance in velocity at higher NR value, the variance in velocity behaviour is reelatively similar for all the NR values.

Figure 4.11 shows the increased number of oscillations for the cell rolling on NR = 30 molecules/µm^{-2}. This information is useful to understand the rolling behavior in the shear flow pertaining to sudden jerks in the rolling motion or a smooth transition of cell rolling. This leads us to the analysis of contact area as a function of P-selectin site density.
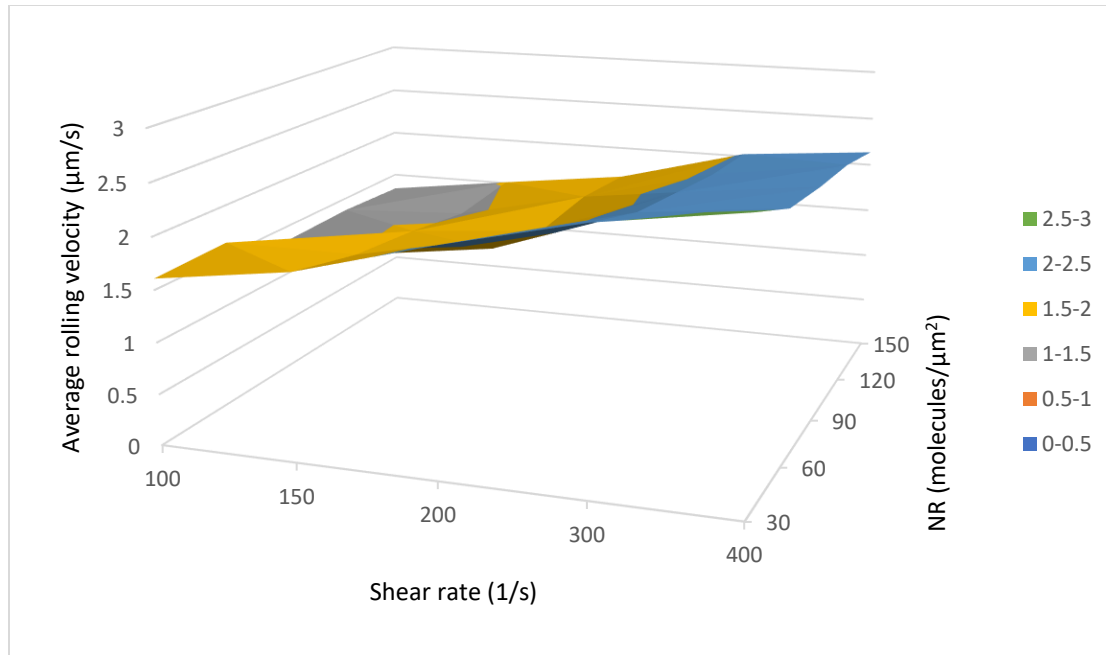
Figure 4.8: The 3D surface area chart shows the average rolling velocity of the capsule as a function of shear rate ranging from 100 to 400 s^{-1} and P-selectin density ranging from 30 to 150 molecules/ µm^{-2}

We also simulated the capsule rolling behavior as a function of shear rate and P-selectin site density. As per our earlier calculations, the surface plot displayed in Figure 4.8 supports our analysis that the rolling velocity of a capsule increases as the shear force is increased, and the rolling velocity of the capsule decreases as the P-selectin site density decreases. We have also determined an equation predicting the rolling velocity based on the trend that we see. This equation is shown here:Rolling velocity = (0.003157708*Shear rate) - (0.003232273* NR) + 1.442511214

4.5: Effect of NR onVariance in instantaneous velocity of capsule in linear shear flow:
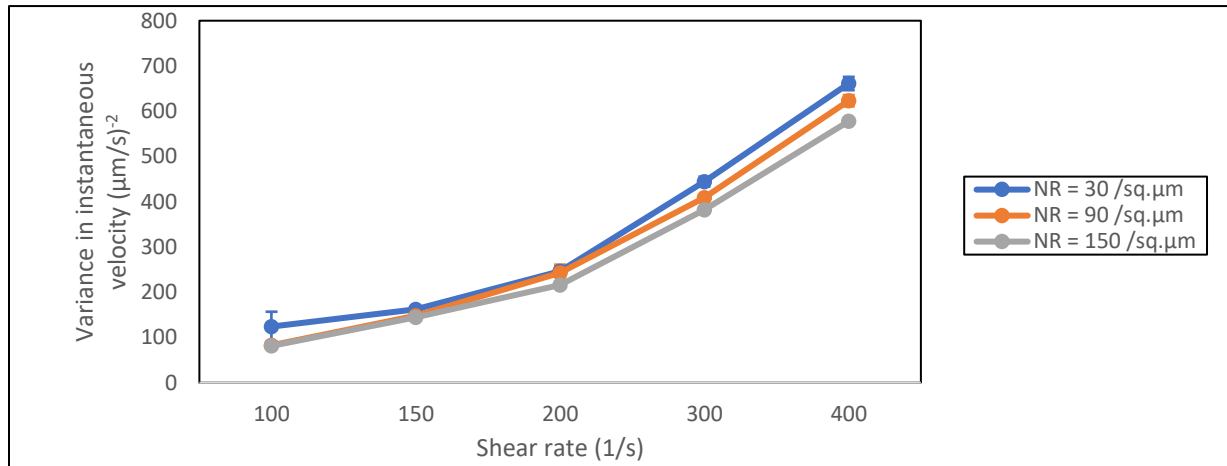
Figure 4.9: The variance in instaneous velocity was computed for the shear rates from 100 to 400 s^{-1} for the P-selectin site density of 30 molecules/µm^{-2}, 90 molecules/µm^{-2} and 150 molecules/µm^{-2}
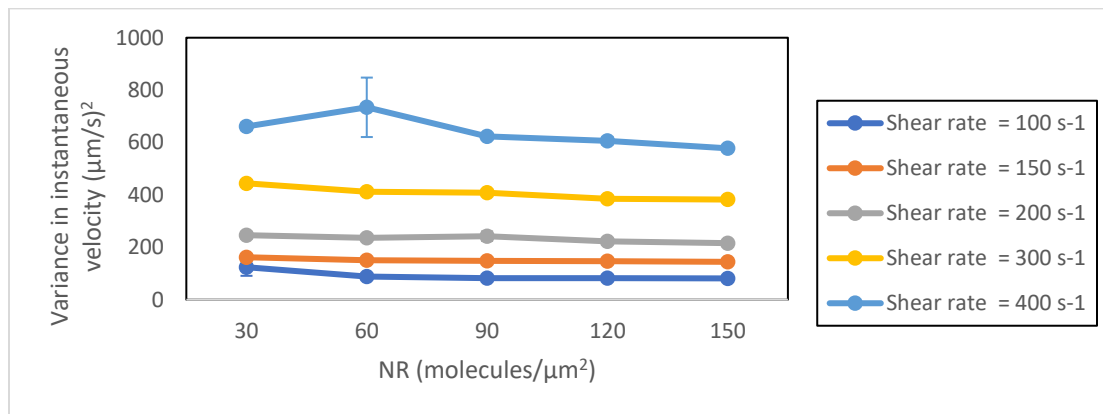
Figure 4.10: The variance in instantaneous velocity is studied as a function of P-selectin site density from 30 molecules/µm^{-2} to 150 molecules/µm^{-2} for shear rate 100 to 400 s^{-1}
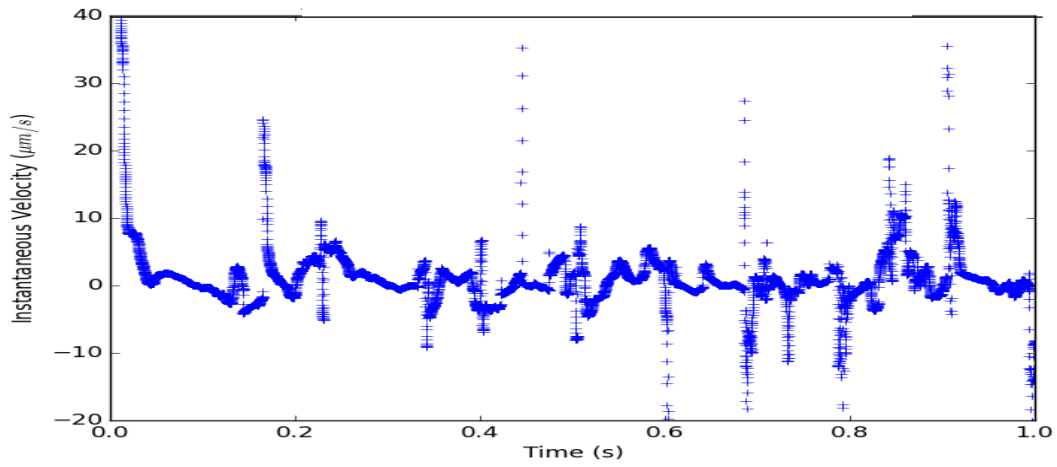
Figure 4.11: The instantaneous rolling velocity of the capsule at a shear rate of 400 s^{-1} was computed for a capsule rolling on a substrate with P-selectin density of 30 molecules/µm^2
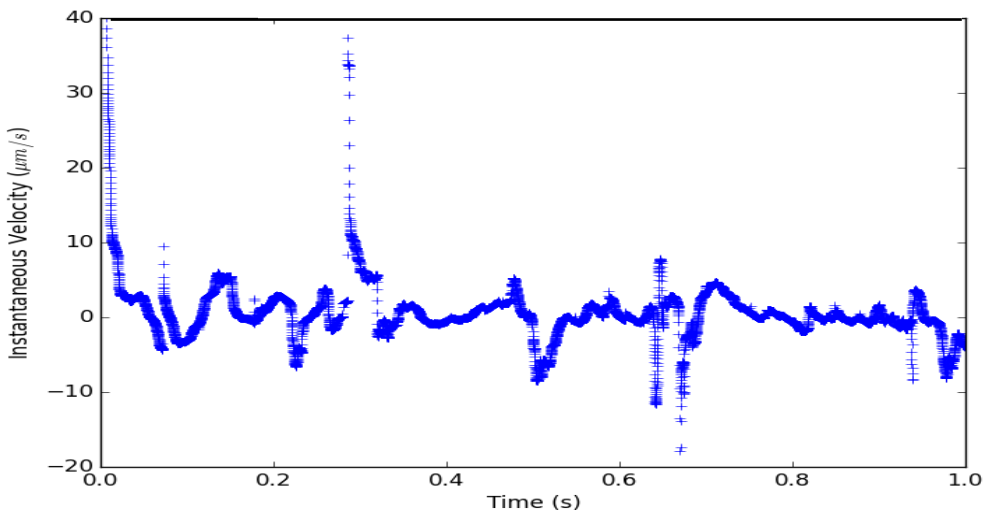
Figure 4.12: The instantaneous rolling velocity of the capsule at a shear rate of 400 s^{-1} was computed for a capsule rolling on a substrate with P-selectin density of 150 molecules/µm^2

4.6 Capsule-substrate contact area under shear flow
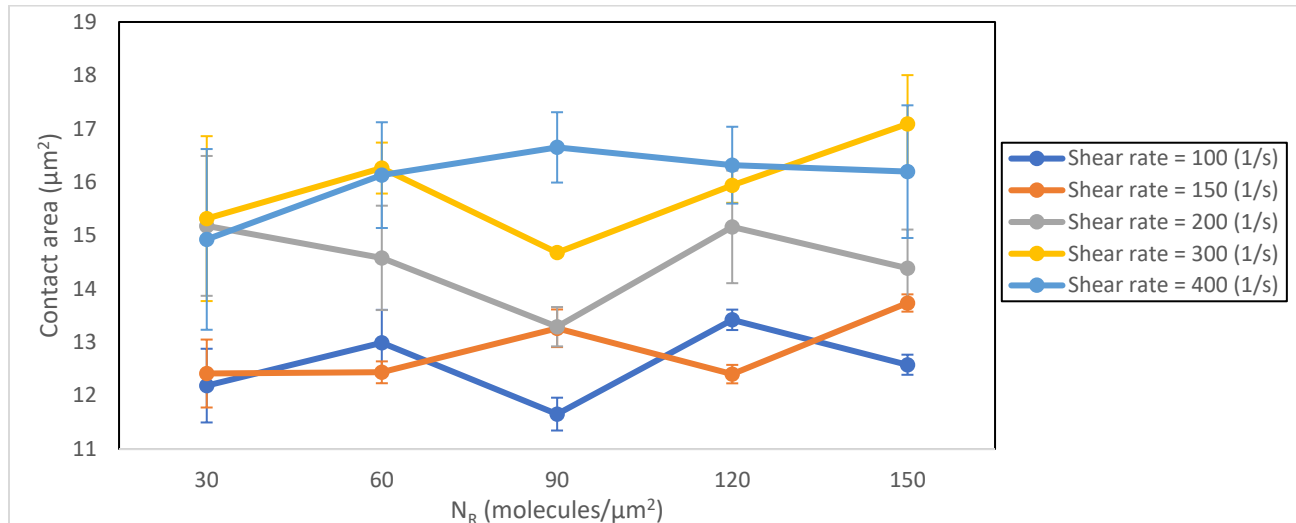
Figure 4.13: Average capsule-substrate contact area as a function of NR from 30 molecules/μm^2 to 150 molecules/μm^2 at shear rates varying from 100 to 400 s^{-1}
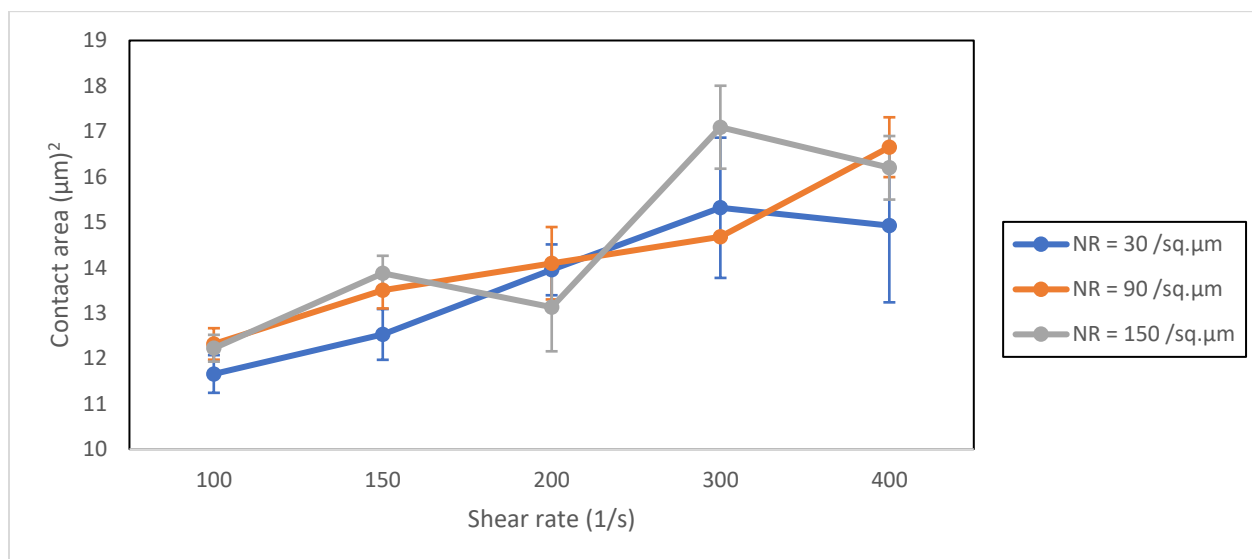
Figure 4.14: Average capsule-substrate contact area as a function of shear rates varying from 100 to 400 s^{-1} at NR 30 molecules/μm^2, 90 molecules/μm^2 and 150 molecules/μm^2

The most prominent reason for the decrease in capsule rolling velocity and rolling velocity variance with higher P-selectin density on the substrate is the increase in bonds formed between the capusle and the substrate. Higher bond formation is associated with higher contact area. The

contact area of the capsule rolling on the substrate coated with various densities of P-selectin is seen in figure 4.13 The contact area for the capsules rolling on a substrate with NR = 150 µm^{-2} is 8% greater than that of the capsule rolling on a substrate with NR = 30 µm^{-2} . As we can see, there is a crossover at NR = 90 µm^{-2} for a shear rate of 400 s^{-1}, this difference is only 3 % which in stochastic analysis negligible and also the value lies in the error bar of NR = 150 µm^{-2} , which means that the difference is insignificant. Thus we can say that the contact area of the capsule rolling on the substrate increases with a higher P selectin density at all values of shear rates.
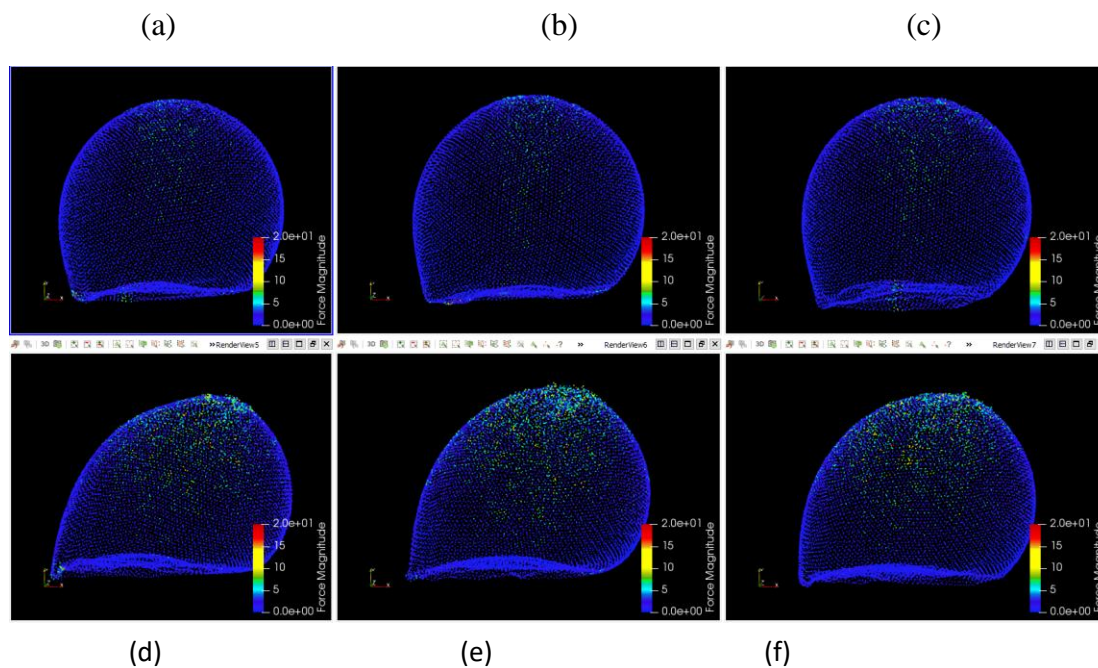
Figure 4.15 a: Shows the contact area shape of the capsule rolling on a surface coated with P-selectin density of 30 molecules/µm^{-2} at shear rate of 100 s^{-1}

Figure 4.15 b: Shows the contact area shape of the capsule rolling on a surface coated with P-selectin density of 90 molecules/µm^{-2} at shear rate of 100 s^{-1}

Figure 4.15 c: Shows the contact area shape of the capsule rolling on a surface coated with P-selectin density of 150 molecules/µm^{-2} at shear rate of 100 s^{-1}

Figure 4.15 d: Shows the contact area shape of the capsule rolling on a surface coated with P-selectin density of 30 molecules/µm^{-2} at shear rate of 400 s^{-1}

Figure 4.15 e: Shows the contact area shape of the capsule rolling on a surface coated with P-selectin density of 90 molecules/μm^{-2} at shear rate of 400 s^{-1}

Figure 4.15 f: Shows the contact area shape of the capsule rolling on a surface coated with P-selectin density of 150 molecules/μm^{-2} at shear rate of 400 s^{-1}

Figure 4.16 (a): Shows the capsule substrate contact area for a capsule rolling on a substrate coated with the NR 30 molecules/ μm^{-2} at a shear rate of 100 s^{-1}

Figure 4.16 (b): Shows the capsule substrate contact area for a capsule rolling on a substrate coated with the NR 30 molecules/ μm^{-2} at a shear rate of 400 s^{-1}
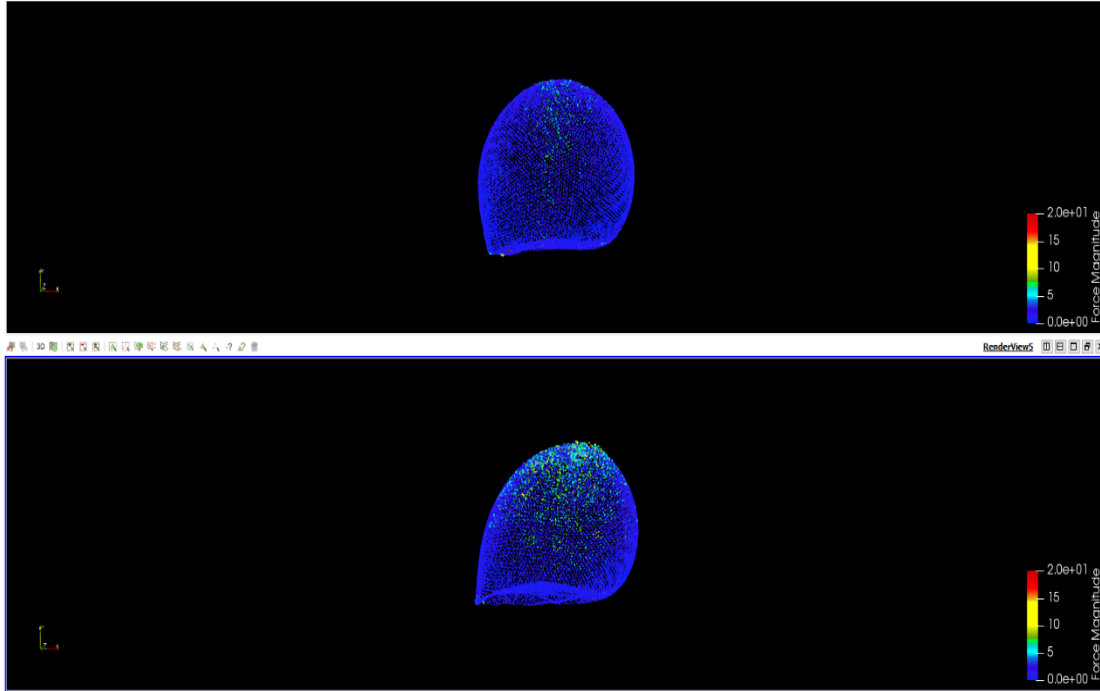
Figure 4.16 (c): Shows the capsule substrate contact area for a capsule rolling on a substrate coated with the NR 90 molecules/ μm^{-2} at a shear rate of 100 s^{-1}

Figure 4.16 (d): Shows the capsule substrate contact area for a capsule rolling on a substrate coated with the NR 90 molecules/ μm^{-2} at a shear rate of 400 s^{-1}
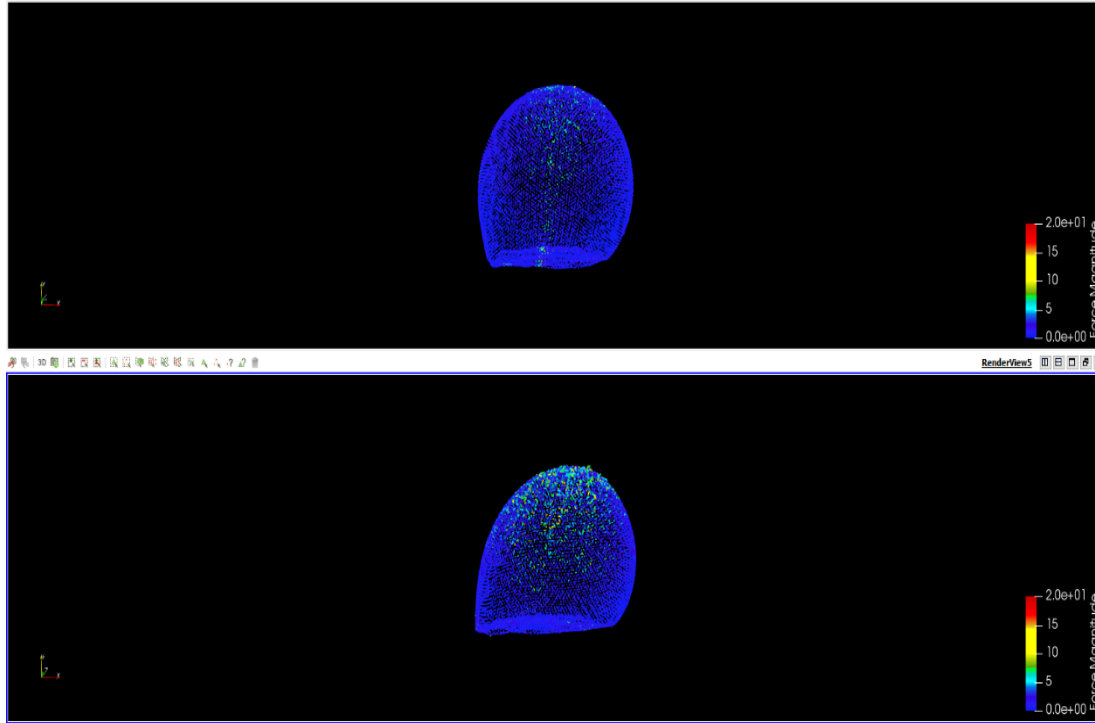
Figure 4.16 (e): Shows the capsule substrate contact area for a capsule rolling on a substrate coated with the NR 150 molecules/ μm^{-2} at a shear rate of 100 s^{-1}
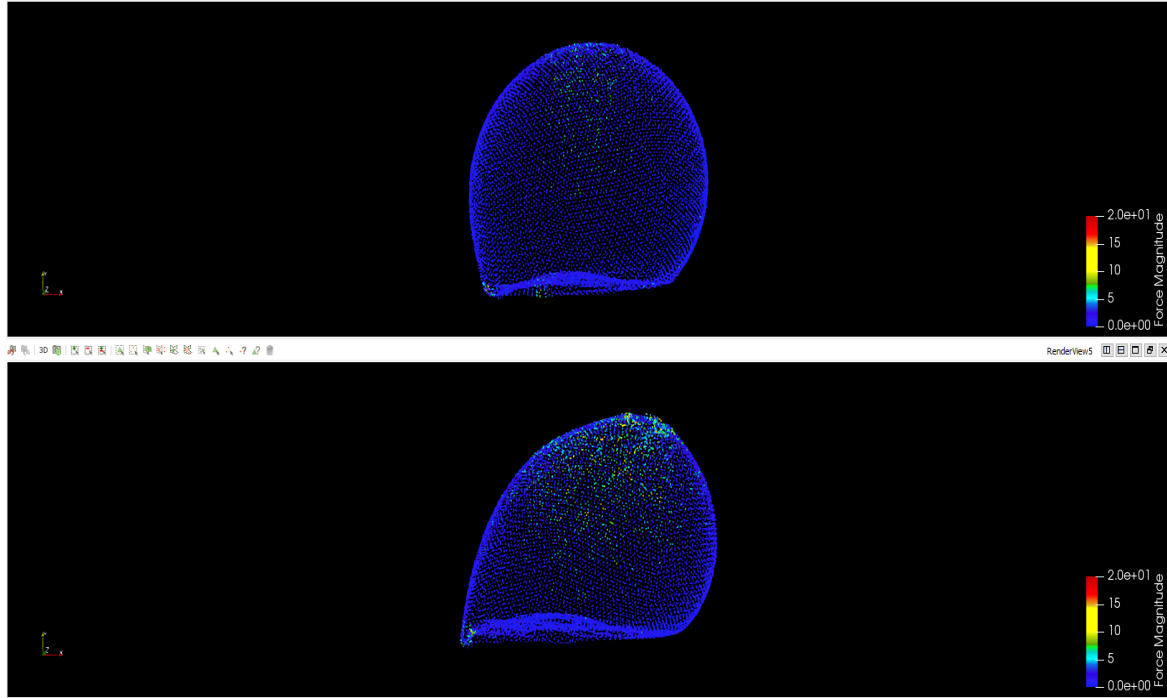
Figure 4.16 (f): Shows the capsule substrate contact area for a capsule rolling on a substrate coated with the NR 150 molecules/ μm^{-2} at a shear rate of 400 s^{-1}

The contact area is the location of adhesion dynamics betweenthe capsule and the substrate. The higher the contact area, the greaterthe number of molecules available to participate in bond formation Increased contact area is associated with increased cell deformation. The contact area of a capsule depends on the shear rate and the P-selectin density. Figure 4.15-Figure 16 depicts the capsule profile in a shear flow field report shear rate. It is observed that at a shear rate of 100 s^{-1} there is a common flattening of the capsule at the region near to the substrate. This flattening is more prominent at a shear rate of 400 s^{-1} . The reason for the increased contact area at a shear rate of 400 s^{-1} is because of an increased hydrodynamic force on the capsule.

4.7 Capsule response to a change in unstressed reverse rate

4.7.a The effect of unstressed reverse on the bond lifetime:

The unstressed reverse rate (Eq. 2.4.4) is dependent on the receptor-ligand bond force, that is determined by the elastic restoring forces in the capsule membrane, the spatial distribution of the bonds and the total number of bonds. Thus, increasing the unstressed reverse rate directly affects the rate of bond dissociation and tends to detach the cell from the substrate We analyzed the effect of unstressed reverse rate constant on the capsule rolling and binding behavior at the highest shear rate of 400 s^{-1} and have presented the results in Figure 4.17. Using the Bell model we have shown the unstressed off rate affects the binding kinetics of the capsule rolling on a substrate coated with P-selectin density ranging from 30 molecules/ μm^{-2} to 150 molecules/ μm^{-2} .The increased unstressed reverse rate is considered to decrease the bond lifetime. Figure 4.14 shows the capsule bond lifetime over a simulation time period of 1 second.The bond lifetime is relatively very high for the capsule at all the P-selectin densities when the unstressed reversed rate is set to 1 s^{-1} compared to when the unstressed reverse rate is set to 25 s^{-1} . The bond lifetime is observed to increase up to 173% on an average when the kro or the unstressed reverse rate is decreased from 25 s^{-1} to 1 s^{-1} .
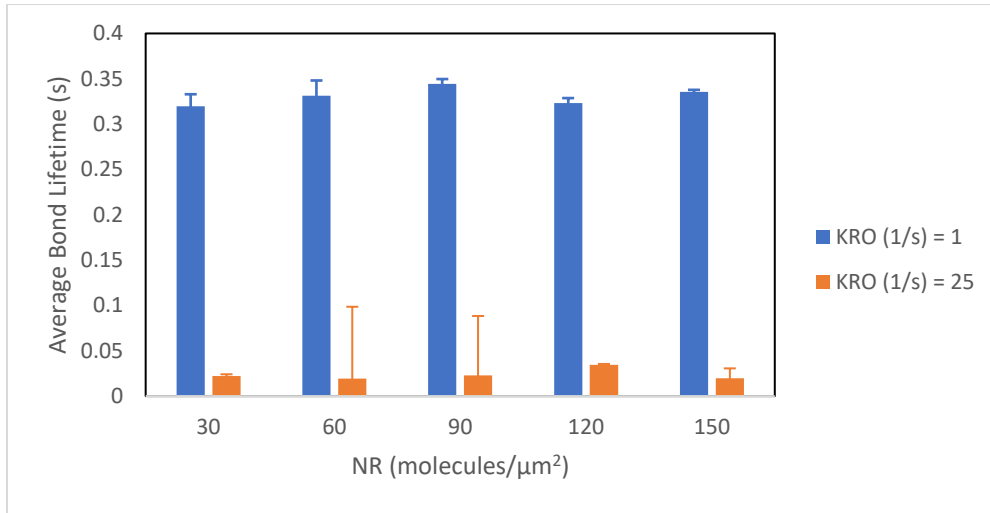

Figure 4.17: Average bond lifetime as a function of P-selectin site density computed for off rate constant KRO $=1$ s^{-1} and 25 s^{-1} at shear rate 400 s^{-1}

4.7.b Effect of unstressed reverse rate on the number of bonds formed:
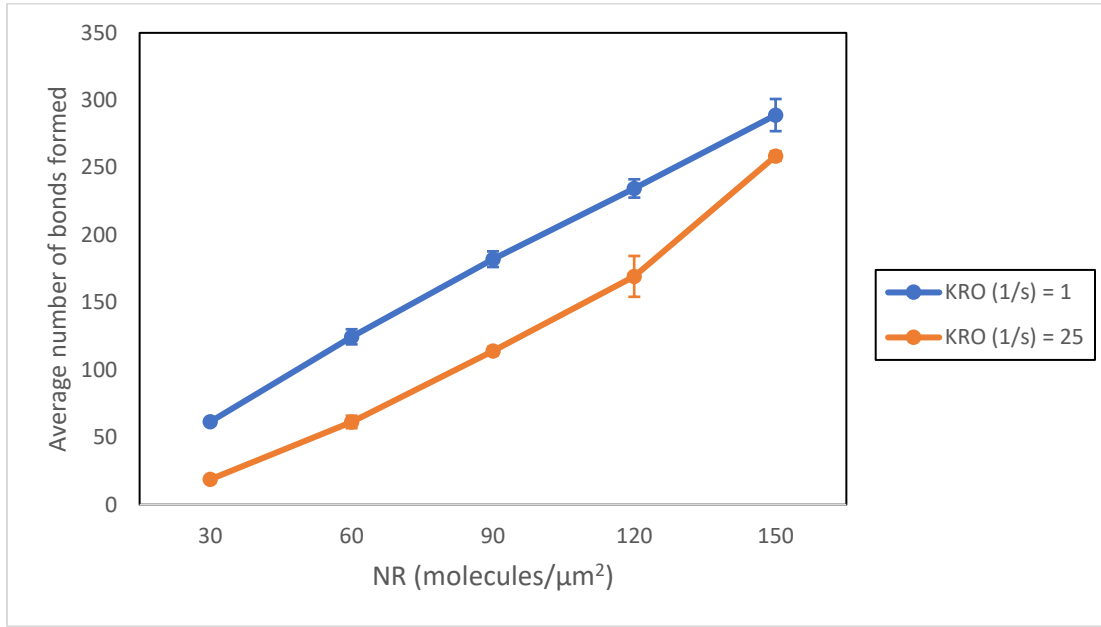
Figure 4.18: Average number of bonds as a function of P-selectin site density computed for off rate constant $k_r^0 = 1$ s^{-1} and 25 s^{-1} at shear rate 400 s^{-1}

We then observed the number of receptor-ligand bonds formed between the capsule and the substrate at a shear rate of 400 s^{-1} and have represented in figure 4.18. The increase in the number of bonds formed for a capsule rolling over a surface with the unstressed reverse rate of 1 s^{-1} was 107% when the P-selectin site density was 30 molecules/µm^2 . This percent difference was observed to be decreasing as we increased the P-selectin density with an increment of 30 molecules/µm^{-2} . Thus, for a capsule rolling on a surface with 60 molecules/ µm^{-2} , the percent difference was 68 %, for 90 molecules/µm^{-2} , for 120 molecules/µm^{-2} the percent difference was 46 % and for 150 molecules/µm^{-2} the percent difference was 32 %. The unstressed reverse rate is directly related with the lifetime of the receptor-ligand complex. It is a first order reaction rate constant. The mean bond lifetime is directly proportional to 1/Kro. Thus the avearge lifespan of a bond is proportional 1/Kro. Shorter bond lifetimes increases the faster capsule rolling on the substrate, since the capsule rolling is faster, the capsule-substrate contact area is lesser. The relatively less contact area proves to make less binding sites available. Thus the number of bonds

formed lessens. Hence it is important to know that, in order to increase the probability of forming receptor-ligand bonds, the unstressed reverse rate needs to be lower.

4.7.c Effect of unstressed reverse rate on the rolling velocity of capsule
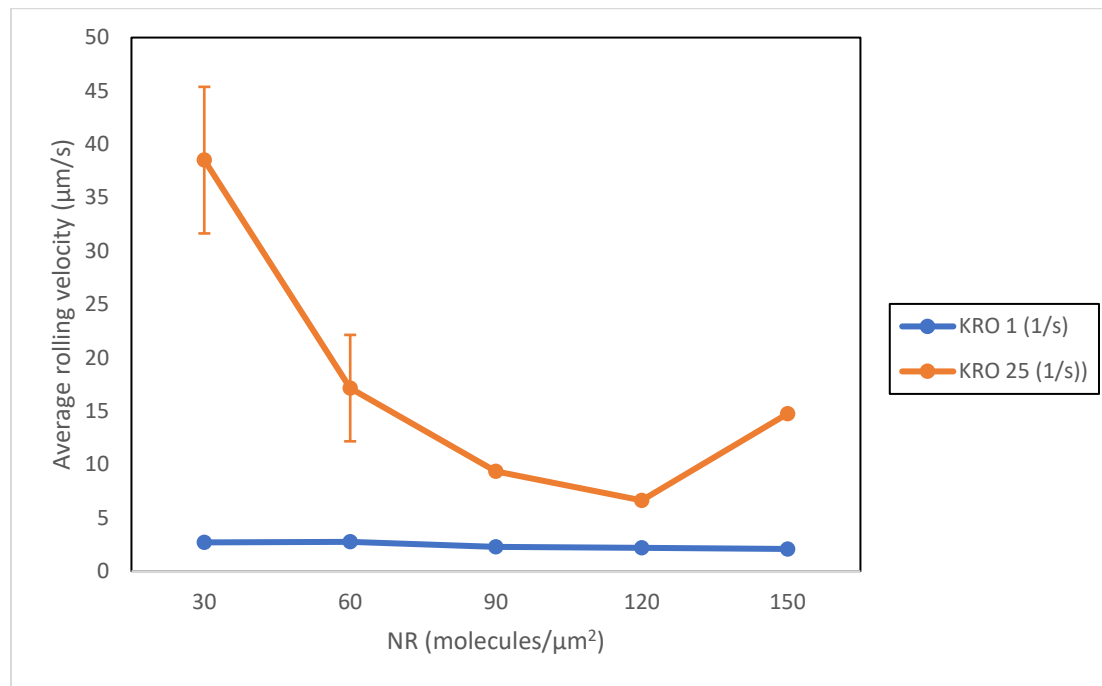
Figure 4.19: Average rolling velocity as a function of P-selectin site density computed for off rate constant KRO =1 s^{-1} and 25 s^{-1} at shear rate 400 s^{-1}

Figure 4.19 represents the capsule rolling behavior on a substrate coated with a range of P-selectin density from 30 molecules/µm^{-2} to 150 molecules/µm^{-2} with an increment of 30 molecules/µm^{-2}. The capsules are observed to roll with an increased rolling velocity at a higher value of the off-rate constant. The percent difference in the rolling velocity is observed to decrease as the P-selectin site density is increased. The percent difference between the rolling velocity of the capsule, rolling on a surface coated with 30 molecules/µm^{-2} at a shear rate of 400 s^{-1} is 174%. The reason for a higher rolling velocity of a capsule at an increased off-rate constant is attributed to the shorter bond lifetime of the capsule at an increased value of off-rate.

4.7.d Effect of unstressed reverse rate on the contact area of capsule
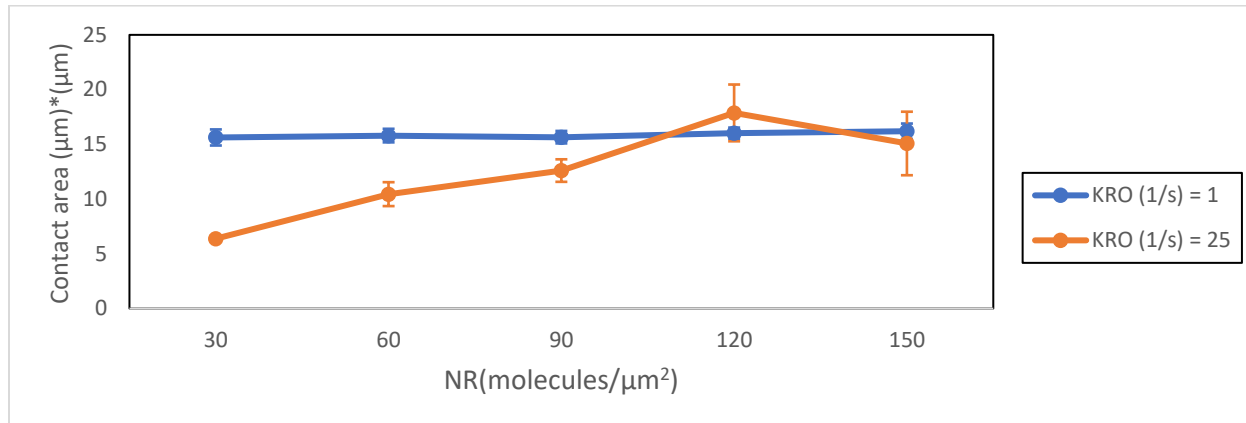
Figure 4.20: Capsule-substrate contact area as a function of P-selectin site density computed for off rate constant KRO =1 s^{-1} and 25 s^{-1} at shear rate 400 s^{-1}

Figure 4.20 represents the capsule contact area with the substrate, as a function of P-selectin site density for different values of unstressed reverse rate constants. An increase in the off-rate constant also known as the reverse rate constant is observed to decrease the contact area of the capsule with the substrate. It is also important to note that this difference is observed to decrease as the P-selectin site density is increased. However, when the P-selectin site density is 120 molecules/µm^2 the rolling velocity of the capsule on the substrate was observed to be slightly greater when the unstressed reverse rate was 25 s^{-1} . The reason for this change in the phenomenon is attributed to the stochastic nature of the kinematics since this increase is 11% and the error bars overlap.

Chapter 5

Conclusions and Future work:

This thesis presented a different perspective on the cell binding and adhesion to the site of inflammation using a computational approach. The focus was on the mechanical behavior of cell rolling on the P-selectin patterned endothelial tissue. The neutrally buoyant capsule was seen to travel parallel to the wall and exhibit a tank-treading behavior when subjected to shear flow. The initially spherical and deformable capsule, when subjected to shear flow, exhibited a tank-treading motion.

This solitary cell rolling study indicates that the number of receptor-ligand bond formation increases with an increase in the P-selectin density .A higher number of bond formation potentially resulted in the slower rolling of the capsule. Thereby concluding that the number of receptors on the endothelial cell did control the number of bonds formed. The capsule with a lesser number of receptor-ligand bond formation rolled with a faster rolling velocity as compared to the capsule which had a greater number of bond attachments. The capsule that rolled with a higher rolling velocity, exhibited a greater instability in it's rolling motion. The variance in velocity increased with a decrease in the P-selectin density. This can be attributed to an increase in the total number of bonds, which results in less force per bond. Thus, the bond is more stable when compared to a higher force per bond or a lower total bond force at lower P-selectin density value.

We can say that, increasing the P-selectin density did not significantly influence the bond lifetime. Increasing the P-selectin density had a major influence on the number of bonds formed and the rolling velocity of the capsule. The unstressed reverse rate did significantly alter the behavior of capsule since it substantially influenced the bond lifetime, rolling velocity and the contact area.

The bond lifetime was observed to be affected with a greater magnitude when the unstressed reverse rate was smaller. Thereby, the bond lifetime was shorter for a higher value of unstressed reverse rate. The bond lifetime directly affects the rolling velocity of the capsule. Thus in order for the cell to roll smoothly and slowly the unstressed reverse rate is suggested to be kept at a smaller value. The capsule-substrate is inversely proportional to the unstressed reverse rate. And thus, the more contact-area results in more number of bonds formed when the unstressed reverse rate is 1 s^{-1}. Also, the capsule with an unstressed reverse rate of 25 s^{-1} had more contact area in the front of

the capsule, whereas the contact area was more at the rear side of the capsule when the unstressed reverse rate was 1 s^{-1}.

This work focused on developing a uniform P-selectin gradient pattern; the patterning of P-selectin molecules is necessary from a monetary point of view. In future, this work can be extended to computationally find a suitable P-selectin density that can be implemented in a microfluidic device. Employing the deformable microvilli criteria can prove to be a major breakthrough while studying the effects of varying P-selectin density since the deformable microvilli are one of the major factors that influence the cell rolling an binding kinetics. The three-dimensional model that we currently have employs the fluid of the same viscosity inside and outside of the capsule, thus there is a scope where we change these fluid viscosities in the future study.

Studying the adhesive interactions of leukocytes subjected to shear flow and rolling on a substrate coated with P-selectin molecules is critical to understand and monitor an inflammatory response (Nalayanda D.D. et al., 2007). In this study we reconfirm the observation that spatial variations of P-selectin molecule expression on endothelial cells control the behavior of interacting leukocytes seen by (Kim MB et. al.,2004).

By performing a computational study, we were able to demonstrate that adhesion molecules patterned and varied on a surface can alter the mechanical response of leukocyte rolling. To that end we performed parametric studies of P-selectin coated surfaces to determine its effects on cell rolling velocity, total bond force, contact area, number of receptor-ligand bonds present for a simulation time of one second. Through the power of numerical models we were also able to isolate the individual components mentioned above to inspect their response behavior to forces, binding kinetics, number of bonds formed, and variance on rolling velocity. These isolated studies are difficult to achieve in vitro, let alone in vivo.

Limited past computational work (Pawar et al.,2008) have also focused on few patterned surfaces with limited variation in P-selectin density. In this study we have used computational tools to show that cell rolling velocity is dominated by densely populated P-selectin surfaces. That is, the cells roll slower on more densely populated surfaces compared to less populated surfaces. The total bond forces on the cell, increase with increased surface densification of P-selectin. The information garnered from this study can be used by engineers in the design of microfluidic devices where gradient patterns of cell can be implemented to study and understand the rolling behavior in these

devices. In fact (Nalayanda D.D. et al., 2007) have demonstrated the feasibility of using microfluidic patterning to fabricate surfaces with well-defined patterns of adhesion molecules.

However, some of the major drawbacks of micro-contact printing on surfaces is that it reduces the concentration of protein that adsorbs on the substrate, since some part of the protein gets adsorbed onto the Polydimethylsiloxane (PDMS) wall of the microfluidic channel. Also, due to the evaporation effects, the protein (eg: P-selectin) gets adsorbed onto that area of the substrate which is not a part of the pattern. These drawbacks result in discrepancies or error in the recorded in vitro data (Nalayanda D.D. et al., 2007).

In light of the aforementioned drawbacks resulting in a lack of precision in recorded data, the computational tool being developed and utilized in this study can be used to conduct these studies as well as aid with more precision, reduction in investment, time, and loss of resources for performing these studies. Finally, the affinity for binding kinetics exhibited in our model can also provide a pathway or insight to understanding the more complex avidity phenomenon that exist in vivo. The work presented here can therefore provide useful data to support and enhance both in vitro/vivo work on leukocyte rolling mechanics.

Bibliography

Bose S.,Singh R., Hanewich-Hollatz M.,Shen C.,Dorfman D.M., Karp J.M., Karnik R. (2013), Affinity flow fractionation of cells via transient interactions with asymmetric molecular patterns, Scientific reports(3), Article number: 2329 (2013)

Balsara H.D., Banton R.J., Eggleton C.D. (2015), Investigating the effects of membrane deformability on artificial capsule adhesion to the functionalized surface, Biomech Model Mechanobiol (2016) 15:1055–1068

Bell, G. I. (1978), Models for the specific adhesion of cells to cells, Science 200(4342), 618-627.

Chen, S. and Springer, T. A. (1999), An automatic braking system that stabilizes leukocyte rolling by an increase in selectin bond number with shear, The Journal
of cell biology 144(1), 185-200.

Chen, S. and Springer, T. A. (2001), Selectin receptor-ligand bonds: Formation limited by shear rate and dissociation governed by the bell model, Proceedings of the National Academy of Sciences 98(3), 950-955.

Charrier, J., Shrivastava, S. and Wu, R. (1989), Free and constrained ination of elastic membranes in relation to thermoforming|non-axisymmetric problems, The Journal of Strain Analysis for Engineering Design 24(2), 55-74.

Chorin, A. (1968), Numerical solution of the Navier-Stokes equations, Mathematics of Computation 22(October 1968), 742-762.

Chorin, A. J. (1969), On the convergence of discrete approximations to the navier-stokes equations, Mathematics of computation 23(106), 341-353.

Damiano, E. R., J. Westheider, A. Tozeren, and K. Ley. 1996. Variation in the velocity, deformation, and adhesion energy density of leukocytes
rolling within venules. Circ. Res. 79:1122–1130.

Dembo, M. (1994), On peeling an adherent cell from a surface, Lectures on Mathematics in the life sciences 24, 51-77.

Dong, X., Tsuda, L., Zavitz, K.H., Lin, M., Li, S., Carthew, R.W., Zipursky, S.L. (1999). ebi regulates epidermal growth factor receptor signaling pathways in Drosophila. Genes Dev. 13(8): 954--965.

Dong, C. and Lei, X. X. (2000), Biomechanics of cell rolling: shear ow, cell-surface

adhesion, and cell deformability., Journal of biomechanics 33(1), 35-43.

Dore, M., Korthuis, R. J., Granger, D. N., Entman, M. L. and Smith, C. W. (1993), P-selectin mediates spontaneous leukocyte rolling in vivo., Blood 82(4), 1308-16.

Eggleton, C. D. and Popel, A. S. (1998), Large deformation of red blood cell ghosts in a simple shear ow, Physics of Fluids (1994-present) 10(8), 1834-1845.

Gupta, V. K., Sraj, I. A., Konstantopoulos, K. and Eggleton, C. D. (2010), Multiscale simulation of l-selectin-psgl-1-dependent homotypic leukocyte binding and rupture., Biomechanics and modeling in mechanobiology 9(5), 613-27.

Hammer, D.A. and Lauffenburger D.A. (1987), A dynamical model for receptor-mediated cell adhesion to surfaces., Biophysical journal, Vol-52, 475-478

Hammer, D. A. and Apte, S. M. (1992), Simulation of cell rolling and adhesion on surfaces in shear flow: general results and analysis of selectin-mediated neutrophil adhesion., Biophysical journal 63(1), 35-57.

Hammer, D. A., Robbins, G. P., Haun, J. B., Lin, J. J., Qi, W., Smith, L. A., Ghoroghchian, P. P., Therien, M. J. and Bates, F. S. (2008a), Leukopolymersomes., Faraday discussions 139, 129-41; discussion 213-28, 419-20.

Hammer, D. A., Robbins, G. P., Haun, J. B., Lin, J. J., Qi, W., Smith, L. A., Ghoroghchian, P. P., Therien, M. J. and Bates, F. S. (2008b), Leukopolymersomes, Faraday discussions 139, 129-141.

Jadhav, S., Eggleton, C. D. and Konstantopoulos, K. (2005), A 3-D Computational Model Predicts that Cell Deformation A_ects Selectin-Mediated Leukocyte Rolling, Biophysical Journal 88(1), 96-104.

Khismatullin, D., Truskey, G., Lawrence, M. and Springer, T. (1991), Three dimensional numerical simulation of receptor-mediated leukocyte adhesion to surfaces: Effects of cell deformability and viscoelasticity., Physics of Fluids 17(3), 859-873.

Khismatullin, Damir B., Truskey, George A., 2012. Leukocyte Rolling on P-Selectin: A Three-Dimensional Numerical Study of the Effect of Cytoplasmic Viscosity. Biophys J 102, 1757-1766.

Khismatullin DB, Truskey GA. A 3D numerical study of the effect of channel height on leukocyte deformation and adhesion in parallel-plate flow chambers. Microvasc Res 68: 188 –202, 2004.

King, M. R., and D. A. Hammer. 2001. Multiparticle adhesive dynamics. Interactions between stably rolling cells. Biophys. J. 81:799–813.

Konstantopoulos K, Kukreti S, McIntire LV. Biomechanics of cell interactions in shear fields. Adv Drug Delivery Res 33: 141–164, 1998.

Krasik, E. F. and Hammer, D. A. (2004), A semianalytic model of leukocyte rolling, Biophysical journal 87(5), 2919-2930.

Lai, M.-C. and Peskin, C. S. (2000), An Immersed Boundary Method with Formal Second-Order Accuracy and Reduced Numerical Viscosity, Journal of Computational Physics 160(2), 705-719.

Lee, Chia-Hua et al. "Steering Trajectories of Rolling Cells by 2D Asymmetric Receptor Patterning." IEEE, 2010. 1–2. Web. 4 Apr. 2012. © 2010 Institute of Electrical and Electronics Engineers

Ley, K. (1996), Molecular mechanisms of leukocyte recruitment in the inammatory process, Cardiovascular Research 32(4), 733-742.

Mayadas, T. N., R. C. Johnson, H. Rayburn, R. O. Hynes, and D. D. Wagner. 1993. Leukocyte rolling and extravasation are severely compromised in P selectin-deficient mice. Cell. 74:541–554.

Mooney, M. (1940), A theory of large elastic deformation., Journal of applied physics Volume pp 11, 582-592.

Nalayanda DD, Kalukanimuttam M., Schmidtke DW, Micropatterned surfaces for controlling cell adhesion and rolling under flow. Biomed Microdevices (2007) 9:207–214

N'Dri, N. A., W. Shyy, and R. Tran-Son-Tay. 2003. Computational modeling of cell adhesion and movement using a continuum-kinetics approach. Biophys. J. 85:2273–86.

Pappu, V., Doddi, S. K. and Bagchi, P. (2008), A computational study of leukocyte adhesion and its effect on ow pattern in microvessels., Journal of theoretical biology 254(2), 483-98

Pawar, P., Jadhav, S., Eggleton, C. D. and Konstantopoulos, K. (2008), Roles of cell and microvillus deformation and receptor-ligand binding kinetics in cell rolling. American Journal of Physiology-Heart and Circulatory Physiology 295(4), H1439-H1450.

Peskin, C. S. (1977), Numerical Analysis of Blood Flow in the Heart, Journal of Computational Physics 25(3), 220-252.

Peskin CS, Mcqueen DM. A 3-dimensional computational method for blood-flow in the heart. 1. Immersed elastic fibers in a viscous incompressible fluid. J Comp Physiol 81: 372– 405, 1989.

Peskin, C. S. (2003), The immersed boundary method, Acta Numerica 11.

Rachik, M., Barthes-Biesel, D., Carin, M. and Edwards-Levy, F. (2006), Identification of the elastic properties of an artificial capsule membrane with the compression test: effect of thickness, Journal of colloid and interface science 301(1), 217- 226.

Rivlin, R. (1948), Large elastic deformations of isotropic materials. iv. further developments of the general theory, Philosophical Transactions of the Royal Society of London A: Mathematical, Physical and Engineering Sciences 241(835), 379-397.

Rosar, M. and Peskin, C. S. (2001), Fluid ow in collapsible elastic tubes: a three dimensional numerical model, New York J. Math 7, 281-302.

Smith, M. L., Smith, M. J., Lawrence, M. B. and Ley, K. (2002), Viscosityindependent velocity of neutrophils rolling on p-selectin in vitro or in vivo., Microcirculation (New York, N.Y. : 1994) 9(6), 523-36.

Szatmary, A. C. (2012), PhD Thesis, Technical report, University of Maryland, Baltimore County.

Tandon, P. and Diamond, S. L. (1998), Kinetics of _ 2-integrin and l-selectin bonding during neutrophil aggregation in shear flow, Biophysical journal 75(6), 3163-3178.

Töozeren, A. and Ley, K. (1992), How do selectins mediate leukocyte rolling in venules, Biophysical journal 63(3), 700-9.

Turitto, V. T. 1982. Blood viscosity, mass transport, and thrombogenesis. Prog. Hemost. Thromb. 6:139–177.

Xiaodong He, Trenton R. Schoeb, Angela Panoskaltsis-Mortari, Kurt R. Zinn, Robert A. Kesterson, Junxuan Zhang, Sharon Samuel, M. John Hicks, Michael J. Hickey and Daniel C. Bullard, 2018, Deficiency of P-Selectin or P-Selectin Glycoprotein Ligand-1 Leads to Accelerated Development of Glomerulonephritis and Increased Expression of CC Chemokine Ligand 2 in Lupus-Prone Mice

Z Li, T Lin, X Wu. (2003), New Cartesian grid methods for interface problems using the finite element formulation,Numerische Mathematik 96 (1), 61-98